# Research on Forearm Lateral Movement and Wrist Swing's Continuous Motion Estimation and Estimation Result Correction

**lei zhang** ( 837654890@qq.com )
Northwestern Polytechnical University

**Research**

**Keywords:** sEMG, BP, DOF, exoskeleton robot

**Posted Date:** September 23rd, 2020

**DOI:** https://doi.org/10.21203/rs.3.rs-78822/v1

# Research on forearm lateral movement and wrist swing's continuous motion estimation and estimation result correction

Lei Zhang

School of Mechanical and Electrical Engineering, Northwestern Polytechnical University, 127 Youyi West Road, Xi'an, Shaanxi Province.

**Abstract**-*Objective*: According to the muscle Hill model to estimate the angle of continuous human movement, existing methods require more parameters, and these parameters are susceptible to the influence of different individuals, so there are often large errors in estimation results. *Methods*: Therefore, Back Propagation (BP) neural network model based on features of surface electromyography (sEMG) and the angle of human movement was established in this paper. By studying the role of muscles in joint rotation, appropriate muscle tissues were selected to place EMG sensors, and the model of sEMG features and joint angle was established. For the problem in which sEMG features couldn't fully reflect all EMG information, an extraction method combining time domain, frequency domain and time-frequency domain features was proposed. Aiming at the problem that the Degrees of Freedom (DOFs) of the forearm lateral movement and the wrist swing were controlled by more muscles, which made the joint angle difficult to predict, a method for correcting the estimation angle error by Kalman filter was proposed. Two DOFs exoskeleton robot was designed, and the established model and prototype were used to perform the tracking experiment. *Results*: The average absolute errors of two DOFs are about 17.6° and 6.9°, respectively. *Conclusion:* The results suggested that BP neural network model designed couldn't only achieve uniform velocity tracking of the upper limb, but also ensured that the angular error was within a reasonable value, which met basic requirements for continuous movement estimation of the human body by sEMG.

**Keywords:** sEMG, BP, DOF, exoskeleton robot

## I Instruction

The current research on continuous movement estimation of limbs mainly focuses on the use of various surface electromyography (sEMG) obtained to estimate the corresponding joint angle [1, 2]. There are two ways to achieve continuous movement estimation based on sEMG: the first is to establish a joint dynamics model that takes sEMG as input and combines with muscle physiology, and then calculate joint torque; the second is to directly establish the regression relationship model of sEMG and joint movement angle [3-8].

The existing biomechanical model is mainly the Hill muscle. In 1938, Hill used the frog's sartorius muscle as an experimental sample to get a model of the relationship between muscle contraction force and speed, known as the Hill muscle model. It simplified the model into three components: contraction, series elasticity and parallel elasticity. It was the first relationship model that could successfully describe the changes of muscle

contraction, and had been developed into a general method for predicting the joint movement angle. For example, Cavallaro *et al.* [9] designed an upper limb exoskeleton robot system. The improved Hill muscle model was used for continuous movement estimation, and a 28-channel signals acquisition instrument was used to obtain sEMG, which realized the estimation of the upper limb angle. Pang *et al.* [10] established the Hill muscle model of finger flexion and extension by acquiring sEMG of the superficial flexor and extensor muscles. The obtained signals were processed by Kalman filter, and their relationship model with angle was established. The experiment was conducted in 5 subjects, and results suggested that designed Hill muscle model could complete the angle estimation of the finger flexion.

Different machine learning algorithms are used to establish the relationship model between sEMG and joint angle. The characteristic is that the process is simple and doesn't involve complex calculations. For example, Xiao *et al.* [11] used the average absolute value, waveform length, zero-crossing points and the number of slope sign changes to extract time domain features, and proposed a gray feature weighted support vector machine to construct models of sEMG and elbow joint angles. Ding *et al.* [12] divided sEMG into redundant and non-redundant sub-vectors, established a state-space motion model, and proposed a closed-loop correction algorithm to predict the angle of the upper limb elbow joint.

The elbow movement is mainly powered by biceps and triceps. The sEMG strength and quality is obviously better than others of upper limb muscle. Existing researches on the estimation of upper limb movement angle mainly focus on the elbow joint. Gui *et al.* [13] proposed a method for estimating upper limb joint angle based on support vector regression and muscle coordination model. The experimental results suggested that the estimation of the elbow joint movement angle could obtain a higher accuracy. Raj *et al.* [14] used EMG sensor electrodes to place on biceps to acquire sEMG. Three different models were used to estimate the angular displacement and angular velocity of the elbow joint during continuous flexion and extension. The test results suggested that the adaptive neuro-fuzzy inference system could obtain the best accuracy among three models. Sommer *et al.* [15] used 3-channel EMG sensors to record biceps, triceps, and radial muscle sEMG, and established an external input autoregressive model to predict the elbow continuous movement angle. Li *et al.* [16] used 4-channel EMG sensors to obtain sEMG of subjects' elbows. Using sEMG as input and joint angle as output, a continuous movement estimation model of elbow joint was established. Xiao *et al.* [17] obtained five time domain features of sEMG from biceps and triceps, including the average absolute value, waveform length, zero-crossing times, number of changes in slope sign, and standard deviation. And the random forest was used to predict the angle of the elbow joint. The results suggested that when the joint rotation angular velocity was 15~180.0°/s, a more accuracy could be obtained.

Existing studies use muscle physiology to establish a joint movement model adopting sEMG as input. It has obvious shortcomings, that is, the model has a complicated structure and contains many physiological parameters that can't be directly measured. Some studies had also achieved certain results in optimizing parameters. For example, Ramos *et al.* [18] optimized the Hill parameters through genetic algorithm and established an improved human elbow joint movement angle estimation model. But it introduced a new problem, namely, the selection and applicability of parameter

optimization algorithms. Other research is mainly to establish the relationship model of the machine learning algorithm of sEMG and the joint angle. And the research mainly focuses on the upper and lower limbs, but upper limbs are less involved except the elbow joint. Because the wrist swing and forearm lateral movement are controlled by multiple groups of muscles, it is difficult to estimate the movement using established relationship model, so there is almost no research on them.

In this paper, the upper limb's two Degrees of Freedom (DOFs) movement intention were identified, and were continuously tracked by the exoskeleton robot. Firstly, the study analyzed the preprocessing method of sEMG; in order to obtain signals information comprehensively, extracted features from the time domain, frequency domain and time-frequency domain; on the basis of studying the shape of upper limbs, designed two DOFs upper limb exoskeleton robot; by analyzing the characteristics of the relationship between sEMG feature and the joint angle, the Back Propagation (BP) neural network model of the two was constructed. Aiming at the problem that the forearm lateral movement and the wrist DOFs were controlled by more muscles, which made the joint angle difficult to predict, a method combining Kalman filter to correct the estimation angle error was proposed. Two DOFs tracking test of upper limbs was carried out to verify the effectiveness of the established BP neural network model with the ability to recognize movement intention.

# II METHODS AND MATERIALS

## A. sEMG acquisition

The 8-channel myoelectric ring (Dting-One) produced by Beech Innovation Company was used to obtain sEMG. It is shown in Figure 1. The signals obtained from every channel were amplified by 700 times and then transmitted by Bluetooth to the computer. Its maximum sampling frequency was 100 Hz. But the test requires the sampling frequency of 1000 Hz, which couldn't meet the requirements and need be improved. The improvement scheme: use the wire to draw 5 signals from the myoelectric ring chip. Specifically, instead of the Bluetooth transmission, the negative electrode and the signal electrode on the chip were directly introduced into the data acquisition card (USB-4704) through the wire, and the acquisition card frequency was set to 1000 Hz. The acquisition card was produced by Advantech.

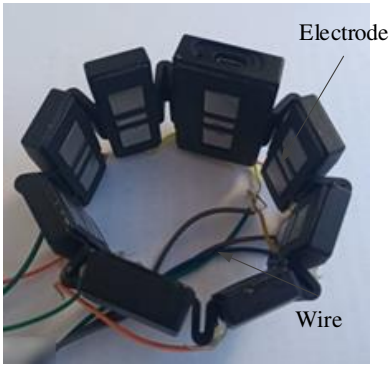


Figure 1 Circumferential electromyography equipment

To extract features from collected data, the data needed to be pre-processed. It included amplification, de-biasing, bandpass filter and Kalman filter. Since the output signals contained 2.5V bias voltage, it was necessary to subtract 2.5V from the obtained signals to eliminate the effect. The filter method adopted was digital bandpass filter. According to literature [19-24], the scope was 20-200 Hz and notch filter was performed.

## B. Features

If the time was more than 250ms, people could recognize the delay. Otherwise, people would not be aware it. To avoid this problem,

the data of 250ms was regarded as a set to get features. It was very important to choose appropriate features to ensure the classification accuracy. [25] discussed the importance of choosing appropriate extraction features methods. This paper used Mean Absolute Value (MAV), Discrete Fourier Transform (DFT), and Wavelet Transform (WT) as features [26, 27].

(1) Mean Absolute Value (MAV)

$$\mathrm{MAV}=\frac{1}{N}\sum_{n=1}^{N}\left|x\ n\right| \quad (1)$$

where, $N$ is the number of sample; $x(n)$ is signals.

(2) Discrete Fourier Transform (DFT)

The Fourier transform converts signals to frequency domain, so researchers can observe information which can't be observed in time domain. sEMG collected are discrete, so DFT is needed for $x(n)$. The transform formulas are defined as

$$\begin{cases} X\ k=\sum_{n=0}^{N-1}x\ n\ W_N^{nk} \\ x\ n=\frac{1}{N}\sum_{k=0}^{N-1}X\ k\ W_N^{-nk} \end{cases} \quad (2)$$

where, $W_N=\mathrm{e}^{-\mathrm{j}\frac{2\pi}{N}}$; $N$ is the number of sample.

(3) Wavelet Transform (WT)

WT is also called "digital microscope". It can observe and analyze the signals from different angles and scales, and decompose it at different frequency. For the signals $x(t)$, the wavelet transform is

$$W_f\ a,b=\frac{1}{\sqrt{a}}\int_{-\infty}^{\infty}x\ t\ \psi_{a,b}\left(\frac{t-b}{a}\right)\mathrm{d}t \quad (3)$$

where, $\frac{1}{\sqrt{a}}\psi_{a,b}\left(\frac{t-b}{a}\right)$ is the selected wavelet sequence; $a$ is the scaling factor; $b$ is the translation factor; $a, b \in \mathbf{R}$ and $a\neq 0$;

C. Kalman filter

Because sEMG were used to predict the joint movement angle, it had a strong nonlinearity, and the angle estimation of the forearm lateral movement and the wrist swing DOFs were controlled by many different types of muscles, and the estimation results had a large error. So the nonlinear Kalman filter was used to modify the estimation result.

The essence of Kalman filter is to estimate the operating state of the system based on the data obtained in the past, and realize the estimation and correction functions. The nonlinear discrete control model is

$$\begin{aligned} \boldsymbol{x}_k &= \boldsymbol{f}_{k-1}\ \boldsymbol{x}_{k-1},\boldsymbol{u}_{k-1},\boldsymbol{w}_{k-1} \\ \boldsymbol{z}_k &= \boldsymbol{h}_h\ \boldsymbol{x}_k,\boldsymbol{v}_k \end{aligned} \quad (5)$$

where, $\boldsymbol{\mu}_k \in \mathrm{R}^r$ is the input matrix of the system; $\boldsymbol{w}_k \in \mathrm{R}^p$ and $\boldsymbol{v}_k \in \mathrm{R}^q$ are Gaussian white noise, and there is no correlation between the two.

The statistical relationship between $w_k$ and $v_k$ are

$$\begin{cases} \mathrm{E}\ \boldsymbol{w}_k=\boldsymbol{q}_k, \mathrm{Cov}\ \boldsymbol{w}_k,\boldsymbol{w}_j=\boldsymbol{Q}_k\delta_{kj} \\ \mathrm{E}\ \boldsymbol{v}_k=\boldsymbol{r}_k, \mathrm{Cov}\ \boldsymbol{v}_k,\boldsymbol{v}_j=\boldsymbol{R}_k\delta_{kj} \\ \mathrm{Cov}\ \boldsymbol{w}_k,\boldsymbol{v}_j=0 \end{cases}$$

where, $R_k$ is a symmetric positive definite matrix; $Q_k$ is a symmetric non-negative definite matrix.

The initial state $x_0$ is independent of $w_k$ and $v_k$. The mean and the covariance matrix of $x_0$ are

$$\begin{cases} \hat{\boldsymbol{x}}_0=\mathrm{E}\ \boldsymbol{x}_0 \\ \boldsymbol{P}_0=\mathrm{Cov}\ \boldsymbol{x}_0,\boldsymbol{x}_0=\mathrm{E}\left[\ \boldsymbol{x}_0-\hat{\boldsymbol{x}}_0\quad \boldsymbol{x}_0-\hat{\boldsymbol{x}}_0\ ^{\mathrm{T}}\right] \end{cases} \quad (7)$$

The nonlinear control model $f_{k-1}(\cdot)$ is expanded into a Taylor series on the basis of the filtered value $\hat{\boldsymbol{x}}_{k-1}$, and the second and higher order are omitted, and $x_k$ is

$$\boldsymbol{x}_k \approx \boldsymbol{f}_{k-1}\left(\hat{\boldsymbol{x}}_{k-1}, \boldsymbol{u}_{k-1}, \boldsymbol{q}_{k-1}\right) + \frac{\partial \boldsymbol{f}}{\partial \hat{\boldsymbol{x}}_{k-1}}\left(\boldsymbol{x}_{k-1} - \hat{\boldsymbol{x}}_{k-1}\right) + \frac{\partial \boldsymbol{f}}{\partial \boldsymbol{w}_{k-1}}\left(\boldsymbol{w}_{k-1} - \boldsymbol{q}_{k-1}\right) \tag{8}$$

where, $f_{k-1}(\cdot)$, $x_{k-1}$ and $w_{k-1}$ are respectively

$$\boldsymbol{f}_{k-1}(\cdot) = \left[ f_{k-1}^1(\cdot) \quad f_{k-1}^2(\cdot) \quad \cdots \quad f_{k-1}^n(\cdot) \right]^{\mathrm{T}}$$

$$\boldsymbol{x}_{k-1} = \left[ x_{k-1}^1 \quad x_{k-1}^2 \quad \cdots \quad x_{k-1}^n \right]^{\mathrm{T}}$$

$$\boldsymbol{w}_{k-1} = \left[ w_{k-1}^1 \quad w_{k-1}^2 \quad \cdots \quad w_{k-1}^p \right]^{\mathrm{T}}$$

$x_k$ binary first order Taylor series $\frac{\partial \boldsymbol{f}}{\partial \hat{\boldsymbol{x}}_{\mathrm{k-1}}}$, $\frac{\partial \boldsymbol{f}}{\partial \boldsymbol{w}_{\mathrm{k-1}}}$, they are

$$\frac{\partial \boldsymbol{f}}{\partial \hat{\boldsymbol{x}}_{\mathrm{k-1}}} = \left.\frac{\partial \boldsymbol{f}_{\mathrm{k-1}}\left(\boldsymbol{x}_{\mathrm{k-1}}, \boldsymbol{u}_{\mathrm{k-1}}, \boldsymbol{w}_{\mathrm{k-1}}\right)}{\partial \boldsymbol{x}_{\mathrm{k-1}}}\right|_{\substack{\boldsymbol{x}_{k-1}=\hat{\boldsymbol{x}}_{k-1} \\ \boldsymbol{w}_{k-1}=\boldsymbol{q}_{k-1}}} = \left[\begin{array}{cccc} \frac{\partial f_{k-1}^1(\cdot)}{\partial x_{k-1}^1} & \frac{\partial f_{k-1}^1(\cdot)}{\partial x_{k-1}^2} & \cdots & \frac{\partial f_{k-1}^1(\cdot)}{\partial x_{k-1}^n} \\ \frac{\partial f_{k-1}^2(\cdot)}{\partial x_{k-1}^1} & \frac{\partial f_{k-1}^2(\cdot)}{\partial x_{k-1}^2} & \cdots & \frac{\partial f_{k-1}^2(\cdot)}{\partial x_{k-1}^n} \\ \vdots & \vdots & & \vdots \\ \frac{\partial f_{k-1}^n(\cdot)}{\partial x_{k-1}^1} & \frac{\partial f_{k-1}^n(\cdot)}{\partial x_{k-1}^2} & \cdots & \frac{\partial f_{k-1}^n(\cdot)}{\partial x_{k-1}^n} \end{array}\right]_{\substack{\boldsymbol{x}_{k-1}=\hat{\boldsymbol{x}}_{k-1} \\ \boldsymbol{w}_{k-1}=\boldsymbol{q}_{k-1}}}$$

$$\frac{\partial \boldsymbol{f}}{\partial \boldsymbol{w}_{\mathrm{k-1}}} = \left.\frac{\partial \boldsymbol{f}_{\mathrm{k-1}}\left(\boldsymbol{x}_{\mathrm{k-1}}, \boldsymbol{u}_{\mathrm{k-1}}, \boldsymbol{w}_{\mathrm{k-1}}\right)}{\partial \boldsymbol{w}_{\mathrm{k-1}}}\right|_{\substack{\boldsymbol{x}_{k-1}=\hat{\boldsymbol{x}}_{k-1} \\ \boldsymbol{w}_{k-1}=\boldsymbol{q}_{k-1}}} = \left[\begin{array}{cccc} \frac{\partial f_{k-1}^1}{\partial w_{k-1}^1} \cdot & \frac{\partial f_{k-1}^1}{\partial w_{k-1}^2} \cdot & \cdots & \frac{\partial f_{k-1}^1}{\partial w_{k-1}^{\mathrm{p}}} \cdot \\ \frac{\partial f_{k-1}^2}{\partial w_{k-1}^1} \cdot & \frac{\partial f_{k-1}^2}{\partial w_{k-1}^2} \cdot & \cdots & \frac{\partial f_{k-1}^2}{\partial w_{k-1}^p} \cdot \\ \vdots & \vdots & & \vdots \\ \frac{\partial f_{k-1}^n}{\partial w_{k-1}^1} \cdot & \frac{\partial f_{k-1}^n}{\partial w_{k-1}^2} \cdot & \cdots & \frac{\partial f_{k-1}^n}{\partial w_{k-1}^p} \cdot \end{array}\right]_{\substack{\boldsymbol{x}_{k-1}=\hat{\boldsymbol{x}}_{k-1} \\ \boldsymbol{w}_{k-1}=\boldsymbol{q}_{k-1}}}$$

Suppose $\frac{\partial \boldsymbol{f}}{\partial \hat{\boldsymbol{x}}_{k-1}} = \boldsymbol{\Phi}_{k,k-1}$, $\frac{\partial \boldsymbol{f}}{\partial \boldsymbol{w}_{k-1}} = \boldsymbol{\Gamma}_{k,k-1}$,

$\boldsymbol{f}_{k-1}\left(\hat{\boldsymbol{x}}_{k-1}, \boldsymbol{u}_{k-1}, \boldsymbol{q}_{k-1}\right) - \frac{\partial \boldsymbol{f}}{\partial \hat{\boldsymbol{x}}_{k-1}}\hat{\boldsymbol{x}}_{k-1} = \boldsymbol{U}_{k-1}$, then the first order linearization of the state function of the nonlinear model can be transformed into

$$\boldsymbol{x}_k \approx \boldsymbol{\Phi}_{k,k-1}\boldsymbol{x}_{k-1} + \boldsymbol{U}_{k-1} + \boldsymbol{\Gamma}_{k,k-1}\left(\boldsymbol{w}_{k-1}\right.$$

After expanding the nonlinear measurement function $h_k(\cdot)$ around the filter value $\hat{\boldsymbol{x}}_{k|k-1}$, and omitting the Taylor series of the second and higher orders, the function $z_k$ is

$$\boldsymbol{z}_{\mathrm{k}} \approx \boldsymbol{h}_{\mathrm{k}}\left(\hat{\boldsymbol{x}}_{\mathrm{k|k-1}}, \boldsymbol{r}_{\mathrm{k}}\right) + \frac{\partial \boldsymbol{h}}{\partial \hat{\boldsymbol{x}}_{\mathrm{k|k-1}}}\left(\boldsymbol{x}_{\mathrm{k}} - \hat{\boldsymbol{x}}_{\mathrm{k|k-1}}\right) + \frac{\partial \boldsymbol{h}}{\partial \boldsymbol{v}_{\mathrm{k}}}\left(\boldsymbol{v}_{\mathrm{k}} - \boldsymbol{\gamma}_{\mathrm{k}}\right) \tag{10}$$

where, $h_k(\cdot)$ and $v_k$ are

$$\boldsymbol{h}_k(\cdot) = \left[ \mathrm{h}_{\mathrm{k}}^1(\cdot) \quad \mathrm{h}_{\mathrm{k}}^2(\cdot) \quad \cdots \quad \mathrm{h}_{\mathrm{k}}^{\mathrm{m}}(\cdot) \right]^{\mathrm{T}}$$

$\boldsymbol{v}_k = \begin{bmatrix} v_k^1 & v_k^2 & \cdots & v_k^q \end{bmatrix}^{\mathrm{T}}$ $\dfrac{\partial \boldsymbol{h}}{\partial \boldsymbol{v}_{\mathrm{k}}}$, they are $z_k$ binary first order Taylor series $\dfrac{\partial \boldsymbol{h}}{\partial \hat{\boldsymbol{x}}_{\mathrm{k|k\text{-}1}}}$,

$$\frac{\partial \boldsymbol{h}}{\partial \hat{\boldsymbol{x}}_{\mathrm{k|k\text{-}1}}} = \left.\frac{\partial \boldsymbol{h}_{\mathrm{k}}\ \ \boldsymbol{x}_{\mathrm{k}}, \boldsymbol{v}_{\mathrm{k}}}{\partial \boldsymbol{x}_{\mathrm{k}}}\right|_{\substack{\boldsymbol{x}_{\mathrm{k}}=\hat{\boldsymbol{x}}_{\mathrm{k|k\text{-}1}} \\ \boldsymbol{v}_{\mathrm{k}}=\boldsymbol{r}_{\mathrm{k}}}} = \left[\begin{array}{cccc} \frac{\partial h_{\mathrm{k}}^1(\cdot)}{\partial x_{\mathrm{k}}^1} & \frac{\partial h_{\mathrm{k}}^1(\cdot)}{\partial x_{\mathrm{k}}^2} & \cdots & \frac{\partial h_{\mathrm{k}}^1(\cdot)}{\partial x_{\mathrm{k}}^n} \\ \frac{\partial h_{\mathrm{k}}^2(\cdot)}{\partial x_{\mathrm{k}}^1} & \frac{\partial h_{\mathrm{k}}^2(\cdot)}{\partial x_{\mathrm{k}}^2} & \cdots & \frac{\partial h_{\mathrm{k}}^2(\cdot)}{\partial x_{\mathrm{k}}^n} \\ \vdots & \vdots & & \vdots \\ \frac{\partial h_{\mathrm{k}}^m(\cdot)}{\partial x_{\mathrm{k}}^1} & \frac{\partial h_{\mathrm{k}}^m(\cdot)}{\partial x_{\mathrm{k}}^2} & \cdots & \frac{\partial h_{\mathrm{k}}^m(\cdot)}{\partial x_{\mathrm{k}}^n} \end{array}\right]_{\substack{\boldsymbol{x}_{\mathrm{k}}=\hat{\boldsymbol{x}}_{\mathrm{k|k\text{-}1}} \\ \boldsymbol{v}_{\mathrm{k}}=\boldsymbol{r}_{\mathrm{k}}}}$$

$$\frac{\partial \boldsymbol{h}}{\partial \boldsymbol{v}_{\mathrm{k}}} = \left.\frac{\partial \boldsymbol{h}_{\mathrm{k}}\ \ \boldsymbol{x}_{\mathrm{k}}, \boldsymbol{v}_{\mathrm{k}}}{\partial \boldsymbol{v}_{\mathrm{k}}}\right|_{\substack{\boldsymbol{x}_{\mathrm{k}}=\hat{\boldsymbol{x}}_{\mathrm{k|k\text{-}1}} \\ \boldsymbol{v}_{\mathrm{k}}=\boldsymbol{r}_{\mathrm{k}}}} = \left[\begin{array}{cccc} \frac{\partial h_{\mathrm{k}}^1(\cdot)}{\partial v_{\mathrm{k}}^1} & \frac{\partial h_{\mathrm{k}}^1(\cdot)}{\partial v_{\mathrm{k}}^2} & \cdots & \frac{\partial h_{\mathrm{k}}^1(\cdot)}{\partial v_{\mathrm{k}}^q} \\ \frac{\partial h_{\mathrm{k}}^2(\cdot)}{\partial v_{\mathrm{k}}^1} & \frac{\partial h_{\mathrm{k}}^2(\cdot)}{\partial v_{\mathrm{k}}^2} & \cdots & \frac{\partial h_{\mathrm{k}}^2(\cdot)}{\partial v_{\mathrm{k}}^q} \\ \vdots & \vdots & & \vdots \\ \frac{\partial h_{\mathrm{k}}^m(\cdot)}{\partial v_{\mathrm{k}}^1} & \frac{\partial h_{\mathrm{k}}^m(\cdot)}{\partial v_{\mathrm{k}}^2} & \cdots & \frac{\partial h_{\mathrm{k}}^m(\cdot)}{\partial v_{\mathrm{k}}^q} \end{array}\right]_{\substack{\boldsymbol{x}_{\mathrm{k}}=\hat{\boldsymbol{x}}_{\mathrm{k|k\text{-}1}} \\ \boldsymbol{v}_{\mathrm{k}}=\boldsymbol{r}_{\mathrm{k}}}}$$

Suppose $\dfrac{\partial \boldsymbol{h}}{\partial \hat{\boldsymbol{x}}_{k|k-1}} = \boldsymbol{H}_k$ ,

$\boldsymbol{h}_k\ \ \hat{\boldsymbol{x}}_{k|k\text{-}1}, \boldsymbol{r}_k\ \ - \dfrac{\partial \boldsymbol{h}}{\partial \hat{\boldsymbol{x}}_{k|k\text{-}1}} \hat{\boldsymbol{x}}_{k|k\text{-}1} = \boldsymbol{y}_k$ , $\dfrac{\partial \boldsymbol{h}}{\partial \boldsymbol{v}_k} = \boldsymbol{\Lambda}_k$ ,

then the first order linearization of the measurement function of the nonlinear system model is

$$\boldsymbol{z}_k \approx \boldsymbol{H}_k \boldsymbol{x}_k + \boldsymbol{y}_k + \boldsymbol{\Lambda}_k \boldsymbol{v}_k - \boldsymbol{r}_k \qquad (11)$$

The methods used to process the obtained angles are: use formula (9) and (11) to convert the state model from nonlinear to linear; and then use the linear basic equations of the discrete system for Kalman filter.

## D. The range of angle

The upper limb exoskeleton robot had more DOFs, and it was difficult to predict all DOFs' movements. The DOFs of the wrist swing and forearm lateral movement were controlled by multiple groups of muscle, it was difficult to obtain the most effective muscle combination. Moreover, the obtained sEMG were relatively weak, and susceptible to external interference, so the angle estimation was difficult. Existing studies involved less on these DOFs. This paper took these DOFs as the research object to expand the application range of continuous movement estimation.

In order to verify the accuracy of the angle estimation, an upper exoskeleton robot was designed and processed, and the error between the estimation and the human motion angle was observed. Before designing the exoskeleton robot structure, the human physiological structure should be studied to determine the appropriate range of DOFs for each joint. In order to ensure the safety of the exoskeleton robot during operation, two DOFs movement range of the upper limb could be

obtained according to ergonomic characteristics. The forearm lateral movement limit was 0~180.0°. That is, when five fingers and the palm open naturally and were placed horizontally, the center of palm back to the ground was called 0°, and the opposite was 180.0°. The wrist swing range was −90.0~90.0°, that is, the collinearity of the palm and the elbow was called 0°; the inward bending of the palm was 90.0°; and the palm abduction was -90.0°.

Different wrist rotation angles varied greatly. In order to avoid injury and meet the consistency requirements of everyone's rotation angle, the range of the wrist swing DOF in my test was set to 0~50.0°. The angle definition of each DOF was shown in Figure 2, and the range selected for testing was shown in Table 1.

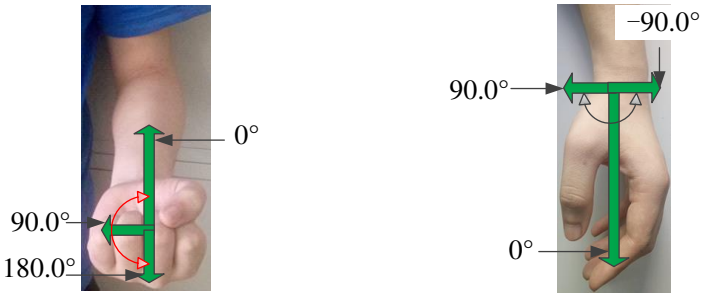


(a) forearm lateral movement angle (b) wrist swing angle

Figure 2 Angle range of each DOF

Table 1 The range of angles selected in the experiment

| Name | Limit range of human movement (° ) | Test angle range (° ) |
|---|---|---|
| Forearm lateral movement DOF | 0~180.0 | 0~180.0 |
| Wrist swing DOF | −90.0~90.0 | 0~50.0 |

## E. Design theory of two DOFs exoskeleton robot

In order to verify the effect of continuous movement estimation on the control of exoskeleton robots, two DOFs exoskeleton robot was designed by comprehensively considering differences in the physiological structure of different upper limbs. In the design process, I mainly considered the following key measures.

(1) Exoskeleton robot skeleton design

The exoskeleton robot needed to be fixed to the upper limb of the subject, and must be designed with a reasonable clamping mechanism so that it could be fixed to the forearm. The overall structural design should be as light as possible under the conditions meeting mechanical requirements. Aluminum alloy 6061 is a high-quality and low-density material produced by heat treatment and pre-stretching. It has the characteristics of good processing performance, no deformation after processing, oxidation resistance and high toughness. Therefore, 6061 was selected as main structural materials. In order to make the overall structure as light as possible, a porous structure was adopted without affecting structural strength. In addition, the installation position of all motors should be considered.

The stepper motor drove the large gear

and small gear to rotate to realize the forearm lateral movement. The test required a low rotation speed and good stability. Therefore, it was necessary to select small modulus gears. The selected gear module was 0.5, finally. The number of teeth of the small gear and the big gear were 90 and 270, respectively. The pitch diameter of the large gear and the small gear are

$$d_1 = mz_1 \tag{12}$$

$$d_2 = mz_2 \tag{13}$$

where, $d_1$ is the small gear's pitch diameter; $d_2$ is the big gear's pitch diameter; $m$ is the modulus; $z_1$ is the teeth number of the small gear; $z_2$ is the teeth number of the big gear.

According to formula (12) and (13), pith diameters were 45.00mm and 135.00mm, respectively. The center distance between the large gear and the small gear is

$$a = \frac{d_1 + d_2}{2} \tag{14}$$

The center distance could be calculated by formula (14), which was 180.00mm. Gears need to be arranged symmetrically, and the material was a soft tooth surface material, and the load variation was small, so the tooth width coefficient $\phi d$ was 0.4. According to the diameter of the dividing circle and the tooth width coefficient, the tooth width $b$ can be obtained as

$$b = \phi_d d_1 \tag{15}$$

According to formula (15), the tooth width of the pinion gear was 18.00mm. Gears are symmetrically arranged, and the large gear was 3~5.00mm narrower than the pinion gear, so the tooth width of the large gear was 13.00mm.

The transmission ratio $N_1$ between the large gear and the small gear was 3. The motor drived the pinion to rotate through the reducer. The gear ratio $N_2$ of the reducer was 5. The relationship between the motor's speed $\omega_0$, rotation angle $\xi_0$ and the large gear's speed $\omega_2$, rotation angle $\xi_2$ are respectively

$$\omega_0 = N_1 N_2 \omega_2 \tag{16}$$

$$\xi_0 = N_1 N_2 \xi_2 \tag{17}$$

(2) Angle sensor

In order to achieve the angle measurement of two DOFs, the corresponding sensor should be selected. Exoskeleton robot's wrist swing and forearm lateral movement angle measurement used a 9-axis attitude sensor (WT901C) with high accuracy and easy installation.

According to the size characteristics of different subjects' upper limbs, a three-dimensional model of the upper limb exoskeleton robot was designed, as shown in Figure 3. Through the strength check, stress analysis and structural optimization, the physical model of the two DOFs upper limb exoskeleton robot was completed, as shown in Figure 4.

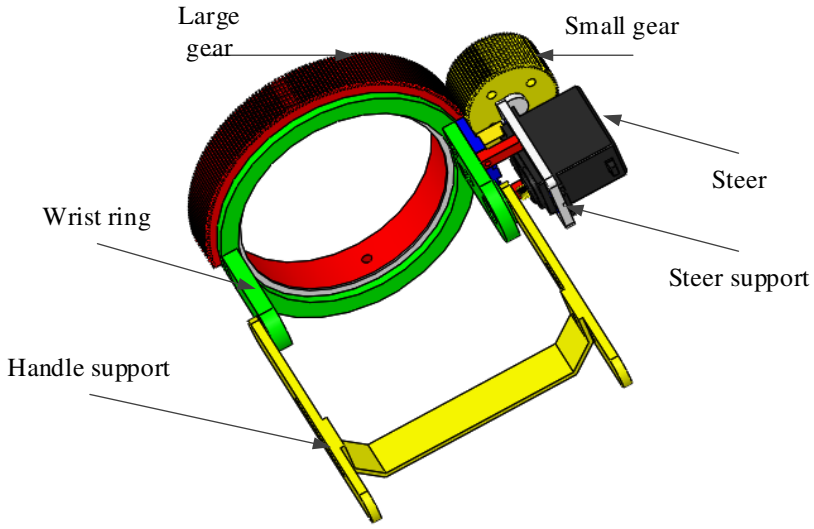


Figure 3 3d drawing of hand support structure

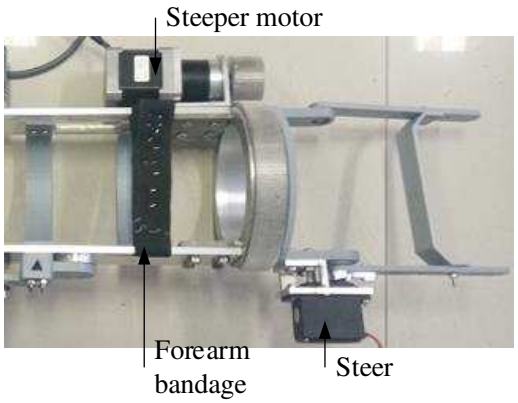


Figure 4 Physical model of exoskeleton robot

## III Results

There was a close relationship between the sEMG of the human body and the movement angle. It was particularly important to choose the appropriate feature extraction method and machine learning algorithm to realize the estimation of human body motion angle. Compared with KNN, LDA and other methods, BP neural network was suitable for the case where the amount of classification data was small and the classification results were large, and because of the small amount of training data in this paper, it was not suitable to use deep learning algorithms. A BP neural network model of sEMG features and motion angles was established to realize the estimation of human motion angles. The input signals of the model were the features of sEMG, and the output signals were the movement angle of the upper limb of human body. The BP neural network used gradient descent to update the weights, which could achieve a faster convergence speed. The training samples of sEMG obtained were $N$ in total, and the total error function $E$ of the samples was

$$E = \frac{1}{2}\sum_{n=1}^{N}\sum_{k=1}^{m} Y_k^{\,n} - O_k^{\,n}\ ^2$$

where, $m$ is the number of nodes in the output

layer; $Y_k^n$ and $O_k^n$ are the expected output and actual output of the $k$-th node in the output layer when the input data is $n$, respectively.

Using gradient descent to update the input layer and hidden layer, the weight $\Delta w_{ij}$ and the threshold $\Delta \gamma_j$ are

$$\Delta w_{ij} = -\eta \frac{\partial E}{\partial w_{ij}} \tag{19}$$

$$\Delta \gamma_j = -\eta \frac{\partial E}{\partial \gamma_j} \tag{20}$$

where, $\Delta w_{ij}$ and $\Delta \gamma_j$ are the weights and threshold correction amounts, respectively.

Then use the above method to update the weight $\Delta v_{jk}$ of the hidden layer and the output layer, and the output layer threshold $\Delta \theta_k$, then

$$\Delta v_{jk} = -\eta \frac{\partial E}{\partial v_{jk}} \tag{21}$$

$$\Delta \theta_k = -\eta \frac{\partial E}{\partial \theta_k} \tag{22}$$

where, $\Delta v_{jk}$ and $\Delta \theta_k$ are the amounts by which the weight and threshold are corrected, respectively.

After the correction, the weights of the input layer and the hidden layer, and the threshold of the hidden layer are

$$w_{ij}^* = w_{ij} + \Delta w_{ij} = w_{ij} - \eta \frac{\partial E}{\partial w_{ij}} \tag{23}$$

$$\gamma_j^* = \gamma_j + \Delta \gamma_j = \gamma_j - \eta \frac{\partial E}{\partial \gamma_j} \tag{24}$$

where, $w_{ij}^*$ and $\gamma_j^*$ are the modified weight and threshold, respectively.

After the correction, the weights of the hidden layer and the output layer $v_{jk}^*$, and the threshold of the output layer $\theta_k^*$ are

$$v_{jk}^* = v_{jk} + \Delta v_{jk} = v_{jk} - \eta \frac{\partial E}{\partial v_{jk}}$$

$$\theta_k^* = \theta_k + \Delta \theta_k = \theta_k - \eta \frac{\partial E}{\partial \theta_k}$$

where, $v_{jk}^*$ and $\theta_k^*$ are the modified weight and threshold, respectively.

Two DOFs were designed for the upper limb exoskeleton robot, and the robot was used to perform two DOFs tracking test. Each DOF of the test had a different placement position and a different rotation angle. It was necessary to establish two models of the relationship between sEMG features and upper limb movement angles. In order to better test the performance of the designed two DOFs relationship model, 8 subjects volunteered to participate. Before the test, keep the electrode sticking site clean and moist; sign an informed consent; at least 2 minutes between each group of movements in the test.

## A. The forearm lateral movement test

According to the relationship between muscles and lateral movement, the electrode placement was pronator teres muscles, flexor carpi radialis, musculi extensor carpi radialis longus, musculi supinator and brachioradialis, as shown in Figure 5. The input layer, the hidden layer and the output layer of the BP neural network has fifteen neurons, six neurons and one neuron, respectively. The transfer functions of hidden layer and output layer were tansig and purelin, respectively; the training number, training speed and target error were 10000, 0.01 and 0.001, respectively [28].

The exoskeleton robot was fixed on the upper limb of an individual who acts as a participant. The attitude sensor lied flat on the

palm of an individual and the x-axis was collinear with the forearm (the individual was the subject). By analyzing the changing of x-axis, the angle of the forearm lateral movement could be obtained. Another attitude sensor was placed on the wrist sleeve of the exoskeleton robot. The x-axis was collinear with the exoskeleton robot's forearm, and the x-axis angle change was analyzed to obtain the rotation angle of the exoskeleton robot's wrist ring. Comparing the difference between two angles, the tracking effect of the forearm lateral movement DOF could be obtained.

During the test, the subject sat on a chair, keeping the body upright and looking straight ahead, and the angle between upper arm and the forearm was 90.0°. Initially, the palm of the subject was parallel to the horizontal plane and the palm was upward, and then rotated 180.0° until the palm was downward. The whole process lasted 5.0s and tried to ensure a constant speed rotation, and other joints were kept as immobile as possible. The palm of the participant was parallel to the horizontal plane and upward, and the forearm was in a relaxed state. During the rotation of the participant's forearm with the exoskeleton robot, DOFs of the other joints should be kept as immobile as possible except for the lateral freedom of movement. The subject's forearm was rotated 180.0° laterally, and the obtained sEMG was used as training data. Extracted features from the data and import them into the BP neural network to generate an angle estimation model, and used the model to predict the lateral rotation angle of human forearm.

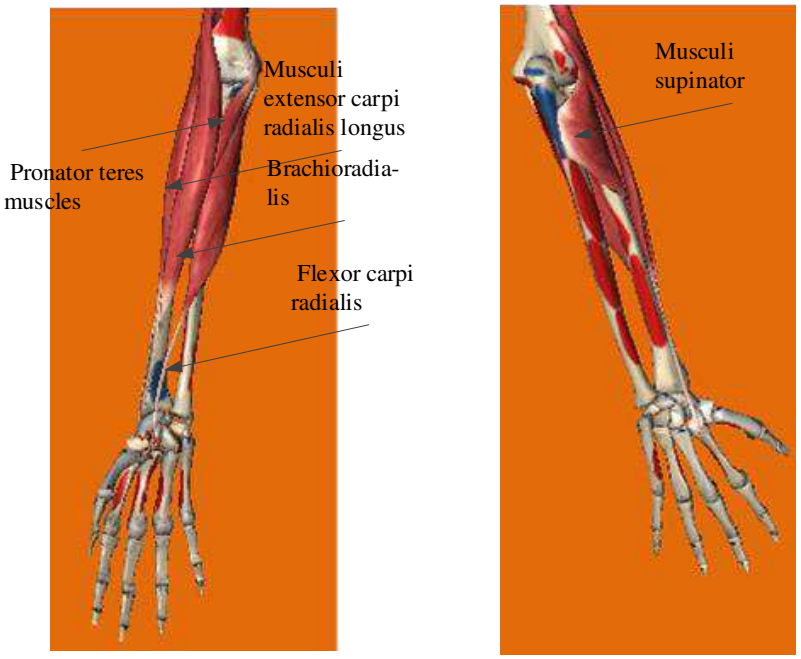


Figure 5 Selected muscle lateral freedom of forearm movement

Used the single chip microcomputer to convert the predicted angle into machine language to complete the control of the motor. Because the DOF of the forearm lateral movement was difficult to predict, the process was offline. After the offline estimation angle was obtained, the Kalman filter was used to correct the error. Imported the correction angle into the single-chip microcomputer to complete the control of the stepper motor of the upper limb exoskeleton robot worn by the participant, and experimental flow was shown in Figure 6.

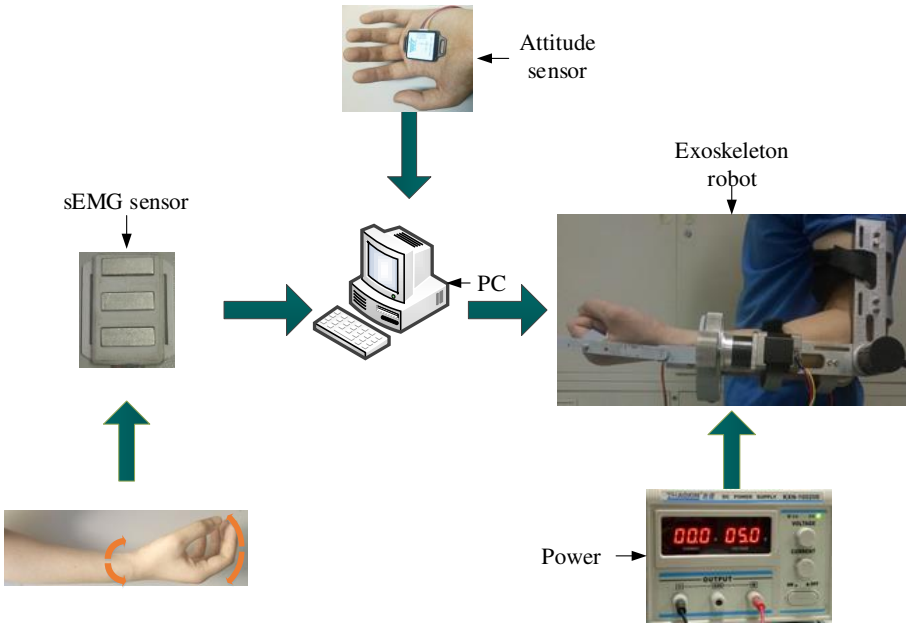


Figure 6 Experimental flow of controlling the exoskeleton robot

Every subject was tested 5 times and results were averaged. Obtained tracking results are shown in Figure 7. Two of subjects tracking results are shown in Figure 8 and Figure 9. Red dashed line represents the lateral rotation angle of the exoskeleton robot obtained with the attitude sensor; blue solid line represents the rotation angle of the human body lateral movement obtained with the attitude sensor, and the difference reflects the tracking error. It can be seen from Figure 7, Figure 8 and Figure 9 that both the tracking effect of the average and the tracking effect of some individual are more accurate and there is no large fluctuation.

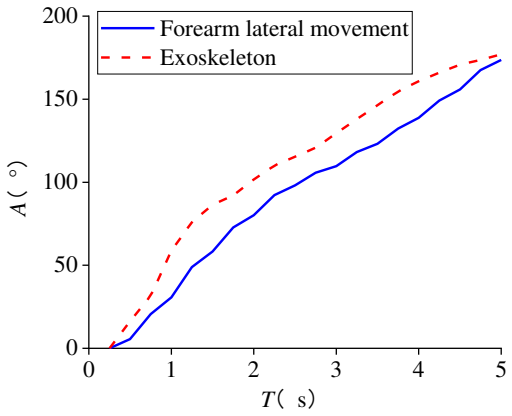


Figure 7 Tracking result of forearm lateral movement DOF

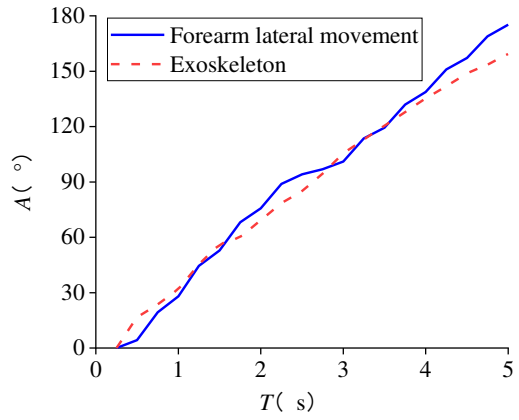


Figure 8 Subject 1 tracking results of forearm lateral movement DOF

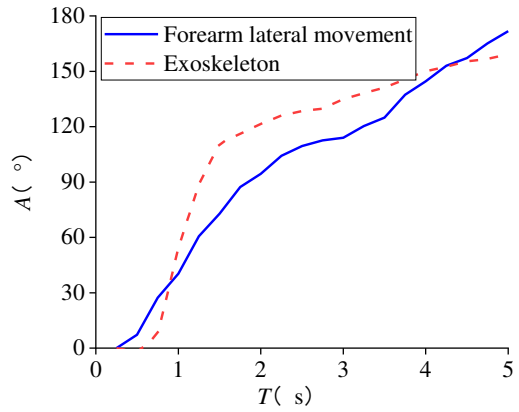


Figure 9 Subject 2 tracking results of forearm lateral movement DOF

The absolute error $\Delta$ and relative error $\delta$ of the joint rotation angle are respectively

$$\Delta = |x_2 - x_1| \tag{27}$$

$$\delta = \frac{|x_2 - x_1|}{x_1} \times 100\% \tag{28}$$

where, $x_1$ is human body joint angle; $x_2$ is exoskeleton robot angle.

I analyzed the error of the obtained tracking results, using formula (28), and obtained the absolute error curve as shown in Figure 10. It can be seen that the error fluctuates around 15.0° during the entire time period, and the average absolute error is about 17.6°.

Using formula (29) to analyze results of the error, in order to avoid that the forearm lateral angle was too small and caused a large relative error, took 1~5.0s to analyze it.

The results are shown in Figure 11. The error at the beginning is relatively large, and finally stabilizes at about 15.0%, and the average value of the relative error is about 23.3%.

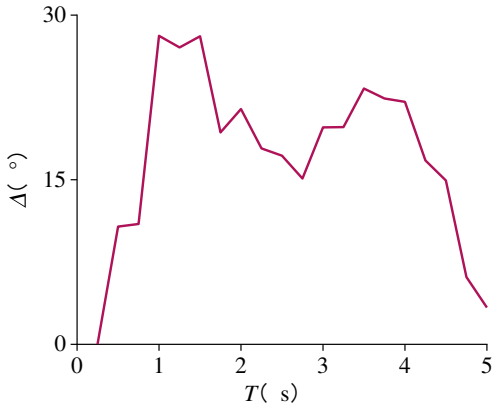


Figure 10 Absolute error curve of forearm lateral movement DOF

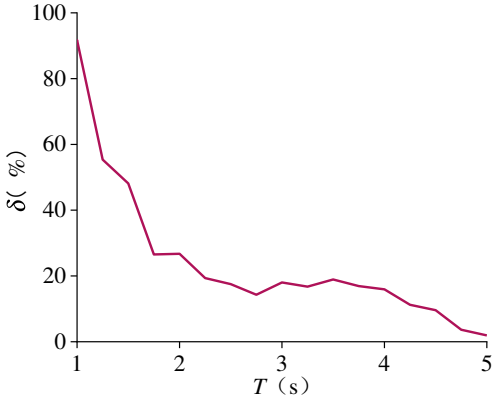


Figure 11 Relative error curve of forearm lateral movement DOF

## B. Wrist swing test

The DOF of the wrist swing is controlled by more muscles, and it is difficult to estimate the continuous movement angle. According to the role of different muscles, after screening, palmaris longus, flexor carpi radialis, musculi extensor carpi radialis longus, extensor carpi ulnaris muscle, and ulnar wrist flexor are used as electrode placement positions. The muscle distribution is shown in Figure 12 . BP neural network was used to build the estimation model, in which there were fifteen neurons in the input layer, six neurons in the hidden layer, and one neuron in the output layer. The exoskeleton robot was fixed on the upper limb of an individual who acted as a participant.

During the test, the attitude sensor was placed on the palm of the other individual, the x-axis was collinear with the forearm, and the y-axis angle of the attitude sensor was the actual rotation angle of the human wrist. Place another attitude sensor on the exoskeleton robot's hand support, the x-axis was collinear with the exoskeleton robot's forearm, and the y-axis angle was the rotation angle of the exoskeleton robot's wrist. Comparing the angle change of the two could get the tracking results.

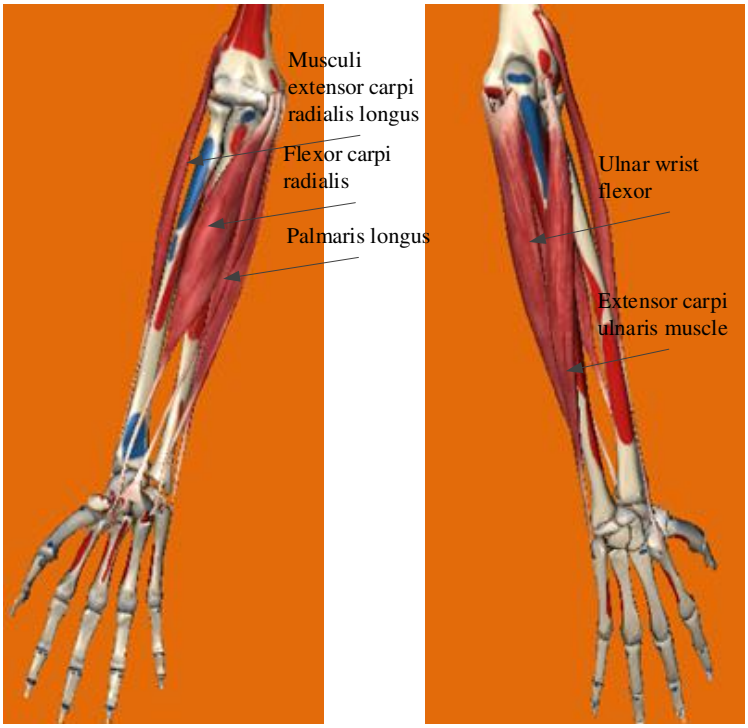


Figure 12 Selected muscles of wrist test

During the test, subject sat on chair, keeping the body upright and looking straight ahead, and upper arm and forearm were at an angle of 90.0°. At the beginning, five fingers of the participant's palm were close together and perpendicular to the horizontal plane, and then rotated 50.0°. The whole rotation process lasted 5.0s, and kept the same speed as possible, and the other joints tried not to move. At the beginning, the participant sat on a chair with an angle of 90.0° between the upper arm and the forearm. Initially, the palm was perpendicular to the horizontal plane and the forearm was in a relaxed state. During the rotation of the exoskeleton robot, other joints except the wrist remain stationary. Selected sEMG of wrist rotation once as training data, extracted features, and imported them into BP neural network to generate angle estimation model, and used the model to predict wrist rotation angle.

The off-line estimation of the DOF of the wrist swing was obtained by sEMG. Based on the offline estimation, Kalman filter was used to modify the estimation angle to reduce the error. Convert the corrected angle into machine language and control the rotation of the wrist servo.

Every subject was conducted 5 times and results were averaged. The obtained tracking results are shown in Figure 13. Two of subjects tracking results of are shown in Figure 14 and Figure 15. The red dashed line represents the wrist rotation angle of the exoskeleton robot obtained with the attitude sensor; the blue solid line represents the rotation angle of the human wrist obtained with the attitude sensor, and the difference reflects the tracking error. It can be seen from Figure 13, Figure 14 and Figure 15 that both the tracking effect of the average and the tracking effect of some individual all change along the increasing direction of the angle, and the trend is consistent with the changing direction of wrist swing.

Using formula (28) to analyze obtained results, results are shown in Figure 16. After analysis, the average absolute error of the whole process is about 6.9°. It can be seen from Figure 13 that the rotation angle of the

human wrist is smaller than that of the exoskeleton robot wrist in the whole process. However, we can see that there is no large fluctuation on the whole from the error curve in Figure 16.

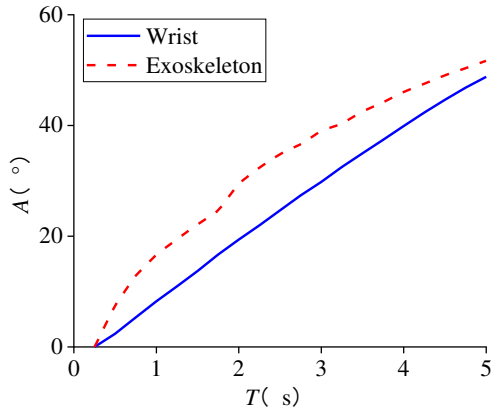


Figure 13 Tracking results of wrist swing DOF

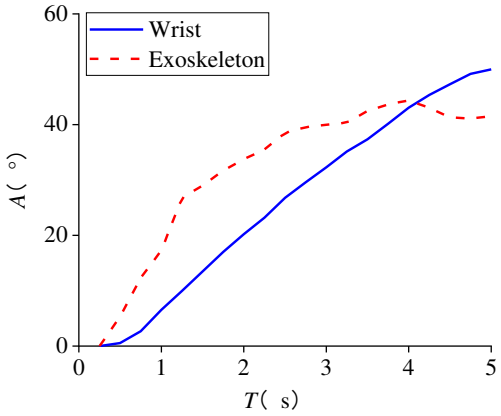


Figure 14 Subject 1 tracking results of wrist swing DOF

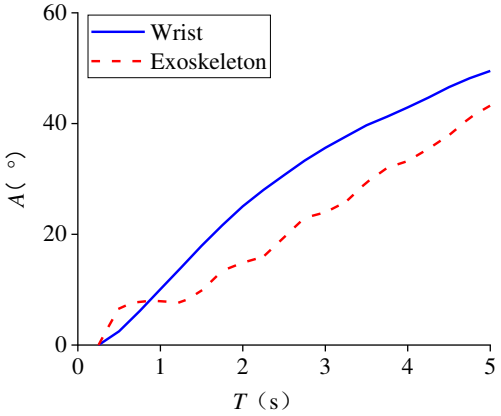


Figure 15 Subject 2 tracking results of wrist swing DOF

Using formula (29) to analyze results of the error, in order to avoid that the wrist angle was too small and caused a large relative error, took 1~5.0s to analyze the relative error, the final results are shown in Figure 17. It can be seen that the error is larger at the beginning, but gradually decreases, and the average relative error is about 35.8%.

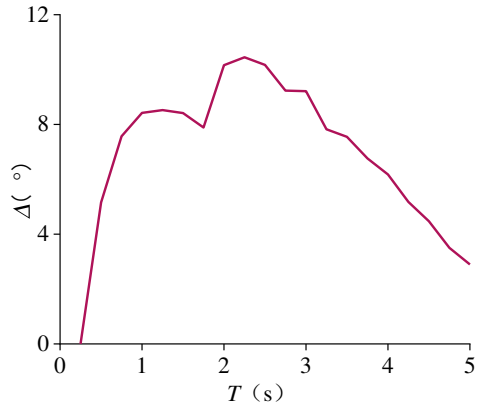


Figure 16 Absolute error curve of wrist swing DOF

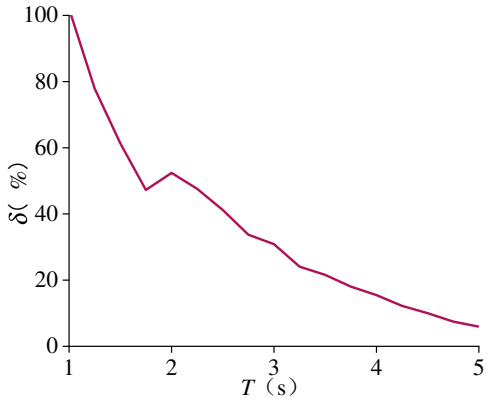


Figure 17 Relative error curve of wrist swing DOF

# IV Discussion and conclusion

## A. Discussion

In this paper, the neural network model was used to avoid the problem of more parameters and optimization of the Hill muscle model. The designed BP estimation model could realize the angle estimation of the forearm: including DOFs of the wrist swing and forearm lateral movement. In order to test the performance of the designed two DOFs continuous movement estimation model, different subjects were selected to participate in the test, and the average absolute and relative errors of results were obtained. The average absolute and relative errors of the forearm lateral movement DOF were about 17.6° and 23.3%, respectively; the average absolute and relative errors of the wrist swinging DOF were about 6.9° and 35.8%, respectively.

In order to estimate the continuous movement of the human body, many scholars had conducted extensive research on this issues. For example, [29] selected the Hill muscle model to predict the continuous movement angle, which improved the estimation accuracy of upper limb motion. Jimson *et al.* [30] established an activation model that parameterizes electromechanical delay artificial neural network by extracting sEMG, estimated the angle of finger joints, and used the estimation results to drive the right-hand index finger exoskeleton robot to evaluate the effect. Because the wrist swing was controlled by multiple groups of muscles, it was difficult to estimate the motion using the established relationship model, so there was almost no research on the wrist. In this paper, the BP neural network model was used

to estimate the rotation angle of the human wrist, expand the freedom range of the upper limb continuous movement estimation, and improve the accuracy of the human-machine collaborative control process of the upper limb exoskeleton robot.

The rotation angle of the forearm lateral movement DOF was 0~180.0°, and the wrist was 0~50.0°. The angle range of forearm lateral movement DOF was the largest, which was 3.6 times of the wrist, but the average absolute error was 2.8 times that of the wrist, so the average absolute error of the forearm lateral movement was smaller than that of the wrist. The average relative error of the wrist swing DOF was also large. Regardless of the subjects' tracking results curve or the average error, the results of wrist swing DOFs were poor, indicating that it was more difficult to predict. Because the wrist was controlled by more muscles, and the muscle volume was relatively small, sEMG were relatively weak, and angle estimation was more difficult. In the later work, methods need to be improved to improve estimation accuracy and achieve online prediction. It can be seen from Figure 7 and Figure 13 that despite the errors, the two DOFs are consistent with the increasing trend of the actual angle, indicating that the errors don't affect the normal rotation control of the exoskeleton robot.

## B. Conclusion

This paper presented the design principles of the two DOFs upper limb exoskeleton robot, and highlighted some structural design methods. The signals preprocessing and features extraction were given. Established the relationship model of sEMG and joint movement angle to realize continuous movement estimation: including the model of forearm lateral movement and wrist swing, and used designed exoskeleton robot to verify the accuracy of the model.

# List of abbreviations

surface electromyography (sEMG)
Degrees of Freedom (DOFs)
Discrete Fourier Transform (DFT)
Wavelet Transform (WT)
Mean Absolute Value (MAV)

## Declarations

### Ethics approval and consent to participate

It was approved by the Medical and Experimental Animal Ethics Committee of Northwestern Polytechnical University.

### Consent for publication

Not applicable

### Availability of data and materials

The datasets used and/or during the current study are available from the corresponding author on reasonable request. All of them signed informed consent forms.

### Competing interests

No conflict of interest exits in the submission of this manuscript, and manuscript is approved by all authors for publication.


### Funding

No funding


### Authors' contributions

L. Zhang completed the research and writing of the paper independently.


### Acknowledgements

Not applicable


### Authors' information (optional)

# V Reference


[1] J. Han *et al.*, "A state-space EMG Model for the Estimation of Continuous Joint

Movements," *IEEE T. Ind. Electron.,* vol. 62, no. 7, pp. 4267-4275, 2015.

[2] Z. Li *et al.*, "Adaptive Impedance Control for an Upper Limb Robotic Exoskeleton Using Biological Signals," *IEEE T. Ind. Electron.,* vol. 64, no. 2, pp. 1664-1674, 2017.

[3] Y. Long *et al.*, "Development and Analysis of an Electrically Actuated Lower Extremity Assistive Exoskeleton," *J. Bionic Eng.,* vol. 14, no. 2, pp. 272-283, 2017.

[4] Y. Kuang *et al.*, "Extreme learning machine classification method for lower limb movement recognition," *Cluster Comput.,* vol. 20, no. 4SI, pp. 3051-3059, 2017.

[5] A. Gijsberts *et al.*, "Movement Error Rate for Evaluation of Machine Learning Methods for sEMG-based Hand Movement Classification," *IEEE T. Neur. Sys. Reh.,* vol. 22, no. 4, pp. 735-744, 2014.

[6] D. Wang *et al.*, "Multi-step ahead electricity price forecasting using a hybrid model based on two-layer decomposition technique and BP neural network optimized by firefly algorithm," *Appl. Energ.,* vol. 190, pp. 390-407, 2017.

[7] Q. Zhang *et al.*, "Simultaneous and Continuous Estimation of Shoulder and Elbow Kinematics from Surface EMG Signals," *Frontiers in Neuroscience,* vol. 11, pp. 2017.

[8] J. M. Hahne *et al.*, "Linear and Nonlinear Regression Techniques for Simultaneous and Proportional Myoelectric Control," *IEEE T. Neur. Sys. Reh.,* vol. 22, no. 2, pp. 269-279, 2014.

[9] E. E. Cavallaro *et al.*, "Real-time Myoprocessors for a Neural Controlled Powered Exoskeleton Arm," *IEEE T. Bio.-Med. Eng.,* vol. 53, no. 11, pp. 2387-2396, 2006.

[10] M. Y. Pang *et al.*, "Finger joint continuous interpretation based on sEMG signals and muscular model," in *IEEE International Conference on Mechatronics and Automation* Takamatsu, 2013, pp. 1435-1440.

[11] F. Xiao *et al.*, "Continuous Estimation of Elbow Joint Angle by Multiple Features of Surface Electromyographic Using Grey Features Weighted Support Vector Machine," *J. Med. Biol. Eng.,* vol. 7, no. 3, pp. 574-583, 2017.

[12] Q. Ding *et al.*, "Continuous Estimation of Human Multi-joint Angles From sEMG Using a State-space Model," *IEEE T. Neur. Sys. Reh.,* vol. 25, no. 9, pp. 1518-1528, 2017.

[13] G. Qizheng *et al.*, "Continuous estimation of upper limb joint motion based on muscle cooperative activation model," *J. Instrum.,* vol. 37, no. 06, pp. 1405-1412, 2016.

[14] R. Raj *et al.*, "Comparative study on estimation of elbow kinematics based on EMG time domain parameters using neural network and ANFIS NARX model," *J. Intell. Fuzzy Syst.,* vol. 32, no. 1, pp. 791-805, 2017.

[15] L. F. Sommer *et al.*, "Elbow Joint Angle Estimation with Surface Electromyography Using Autoregressive Models," in *International Conference of the IEEE Engineering in Medicine and Biology Society*. Honolulu, 2018.

[16] K. X. Li *et al.*, "A novel method for estimating continuous motion and time-varying stiffness of human elbow joint," in *IEEE International Conference on Robotics and Biomimetics*, Kuala Lumpur, 2018, pp. 299-304.

[17] F. Xiao *et al.*, "Continuous estimation of joint angle from electromyography using multiple time-delayed features and random forests," *Biomed. Signal Proces.,* vol. 39, pp. 303-311, 2018.

[18] J. L. A. S. Ramos *et al.*, "Use of Surface Electromyography for Human Amplification Using an Exoskeleton

Driven by Artificial Pneumatic Muscles," in *5th IEEE RAS/EMBS International Conference on Biomedical Robotics and Biomechatronics* Sao Paulo, 2014, pp. 585-590.

[19] K. Englehart *et al.*, "A wavelet-based continuous classification scheme for multifunction myoelectric control," *IEEE T. Bio.-Med. Eng.,* vol. 48, no. 3, pp. 302-311, 2001.

[20] T. Matsubara *et al.*, "Bilinear modeling of EMG signals to extract user-independent features for multiuser myoelectric interface," *IEEE T. Bio.-Med. Eng.,* vol. 60, no. 8, pp. 2205-2213, 2013.

[21] Z. Li *et al.*, "Boosting-Based EMG Patterns Classification Scheme for Robustness Enhancement," *IEEE J. Biomed. Health,* vol. 17, no. 3, pp. 545-552, 2013.

[22] A. J. Young *et al.*, "Classification of Simultaneous Movements Using Surface EMG Pattern Recognition," *IEEE T. Bio.-Med. Eng.,* vol. 60, no. 5, pp. 1250-1258, 2013.

[23] Y. Long *et al.*, "PSO-SVM-Based Online Locomotion Mode Identification for Rehabilitation Robotic Exoskeletons," *Sensors-Basel,* vol. 16, no. 9, pp. 1408, 2016.

[24] Z. Li *et al.*, "sEMG-Based Joint Force Control for an Upper-Limb Power-Assist Exoskeleton Robot," *IEEE J. Biomed. Health,* vol. 18, no. 3, pp. 1043-1050, 2014.

[25] A. Phinyomark *et al.*, "Feature reduction and selection for EMG signal classification," *Expert Syst. Appl.,* vol. 39, no. 8, pp. 7420-7431, 2012.

[26] D. Yang *et al.*, "Experimental Study of an EMG-Controlled 5-DOF Anthropomorphic Prosthetic Hand for Motion Restoration," *J. Intell. Robot. Syst.,* vol. 76, no. 3-4, pp. 427-441, 2014.

[27] T. S. Buchanan *et al.*, "Neuromusculoskeletal modeling: Estimation of muscle forces and joint moments and movements from measurements of neural command," *J. Appl. Biomech.,* vol. 20, no. 4, pp. 367-395, 2004.

[28] J. Chen *et al.*, "Surface EMG based continuous estimation of human lower limb joint angles by using deep belief networks," *Biomed. Signal Proces.,* vol. 40, pp. 335-342, 2018.

[29] J. Han *et al.*, "A state-space EMG Model for the Estimation of Continuous Joint Movements," *IEEE T. Ind. Electron.,* vol. 62, no. 7, pp. 4267-4275, 2015.

[30] J. Vogel *et al.*, "Continuous robot control using surface electromyography of atrophic muscles," in *IEEE International Conference on Intelligent Robots and Systems*, N. Amato, Ed. NEW YORK: IEEE, 2013, pp. 845-850.

# Figures

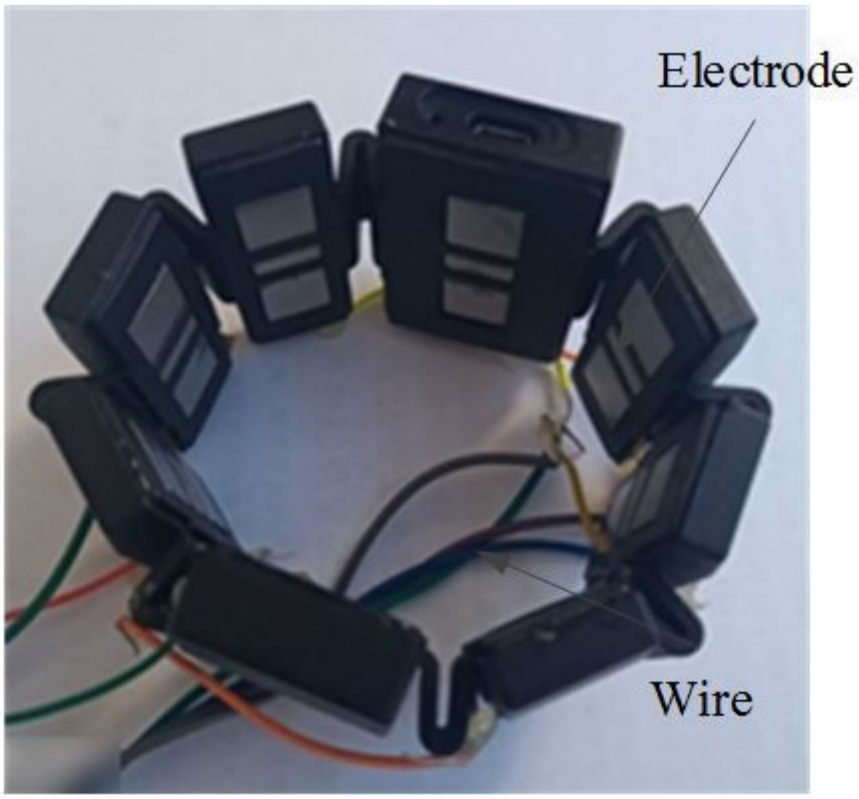


**Figure 1**

Circumferential electromyography equipment

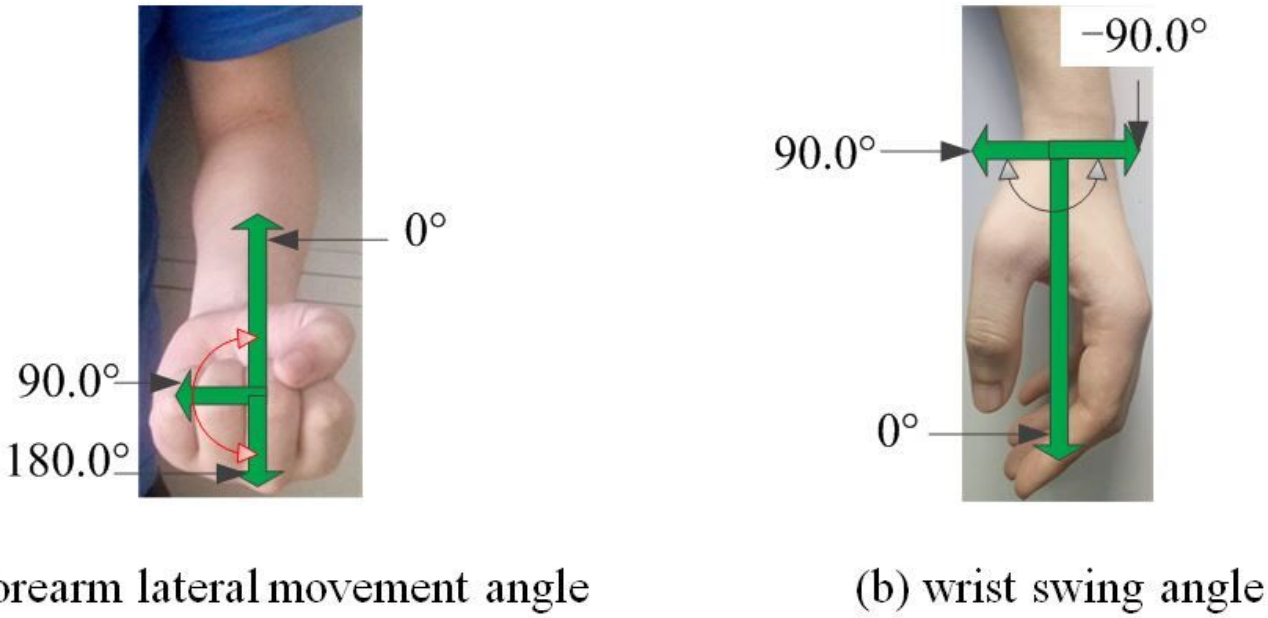


**Figure 2**

Angle range of each DOF

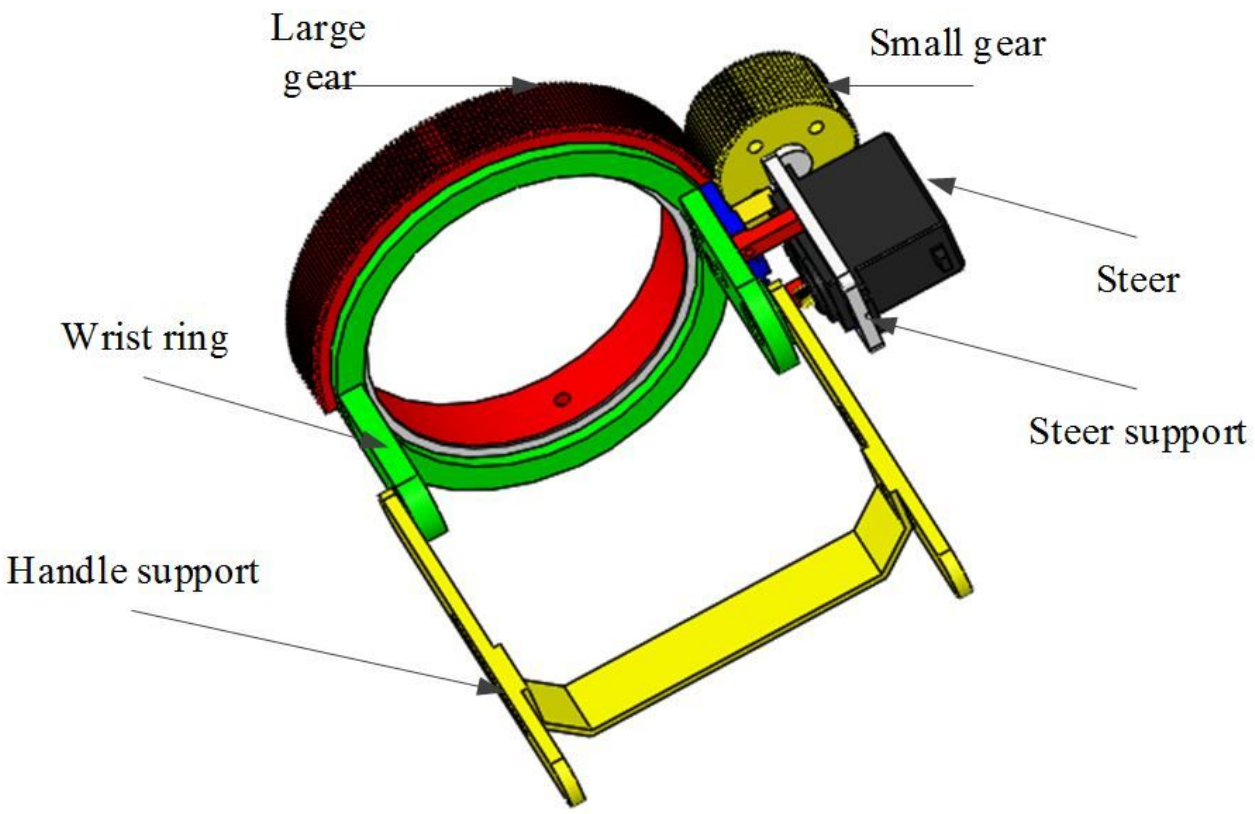


**Figure 3**

3d drawing of hand support structure

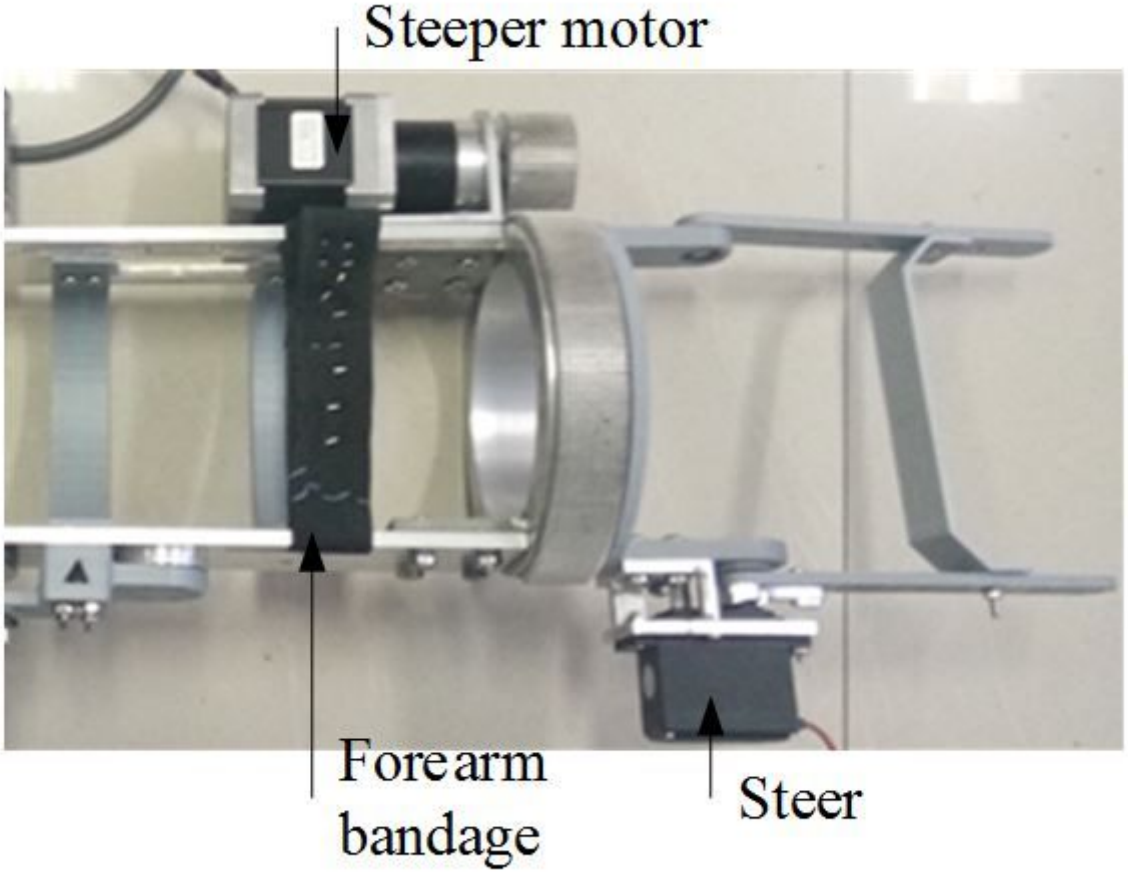


**Figure 4**

Physical model of exoskeleton robot

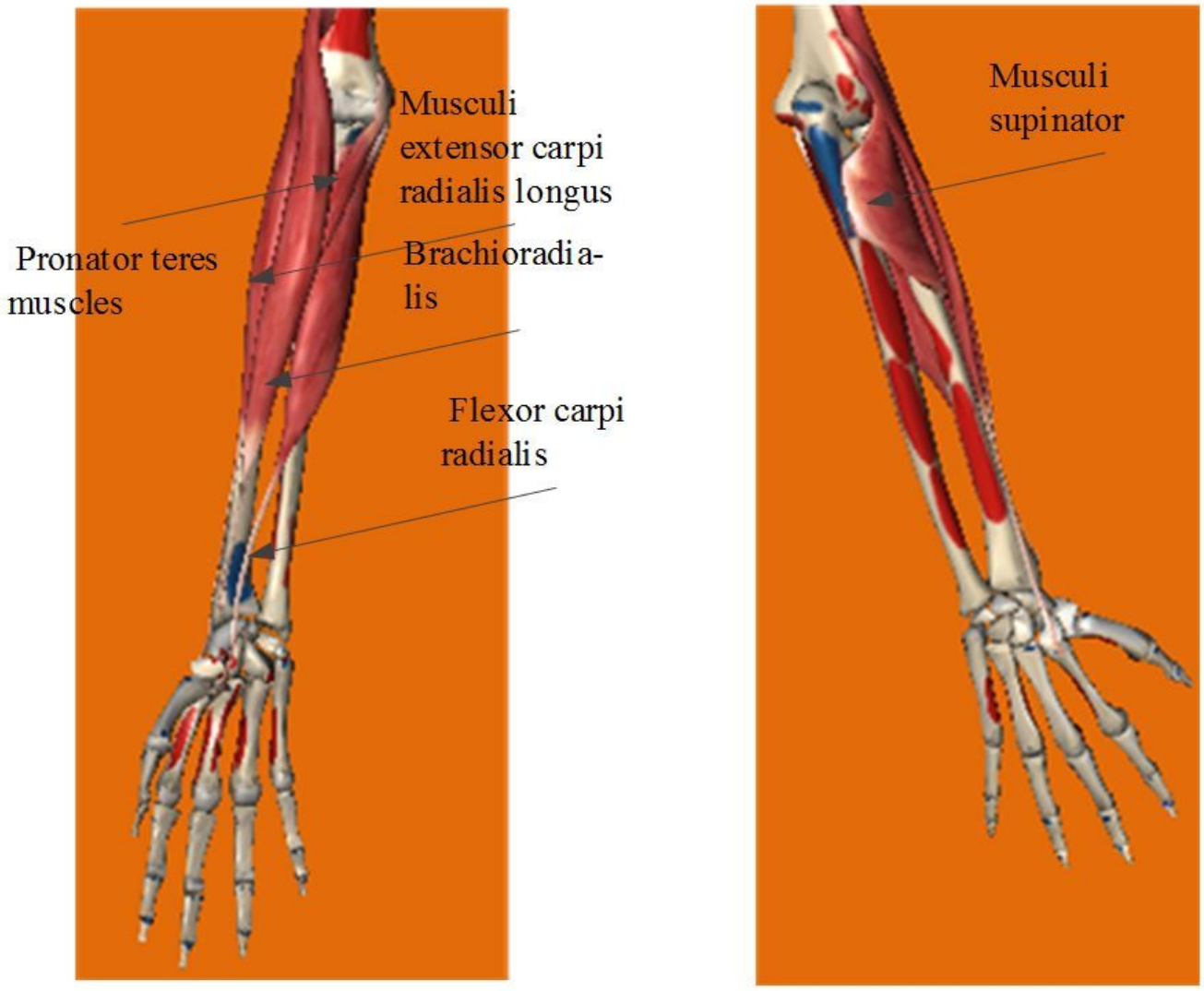


**Figure 5**

Selected muscle lateral freedom of forearm movement

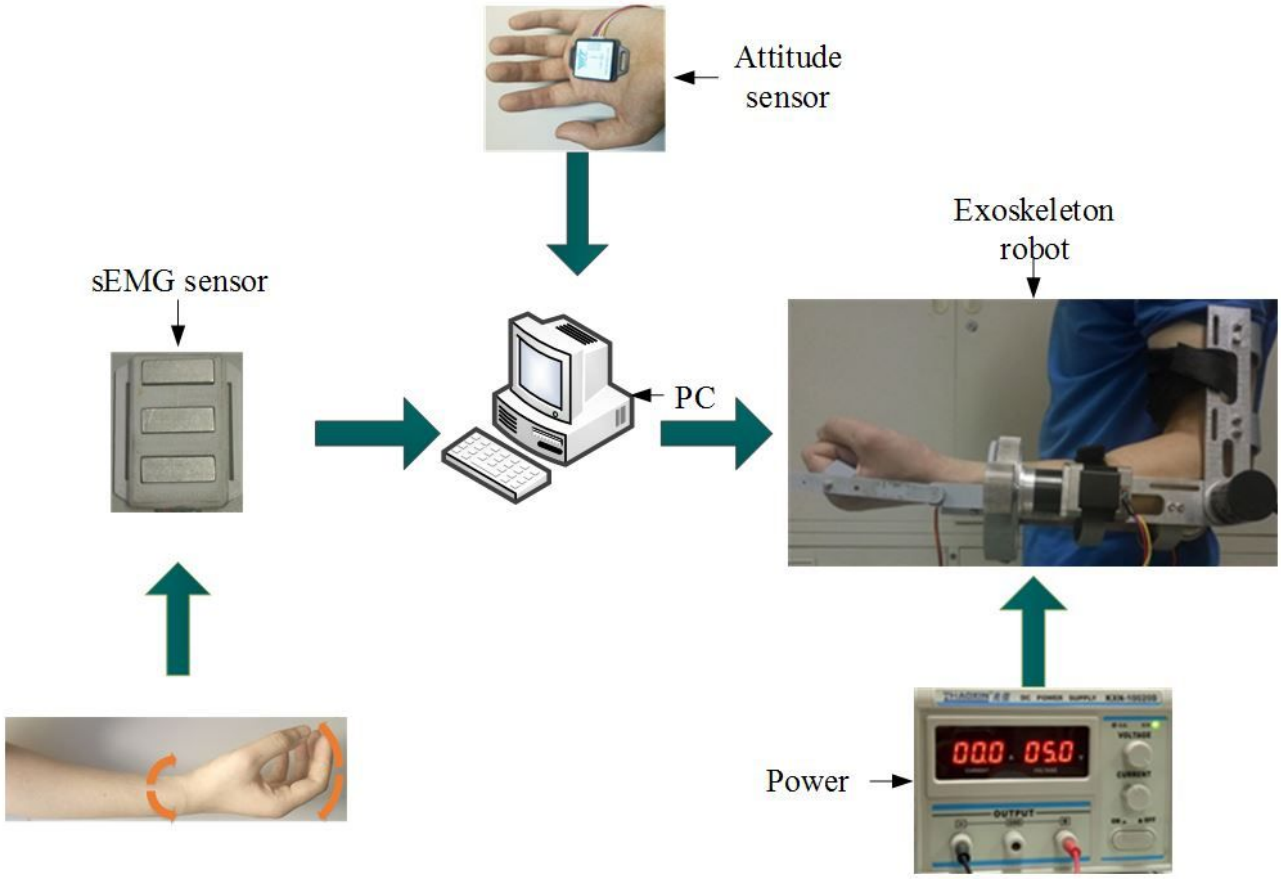


**Figure 6**

Experimental flow of controlling the exoskeleton robot

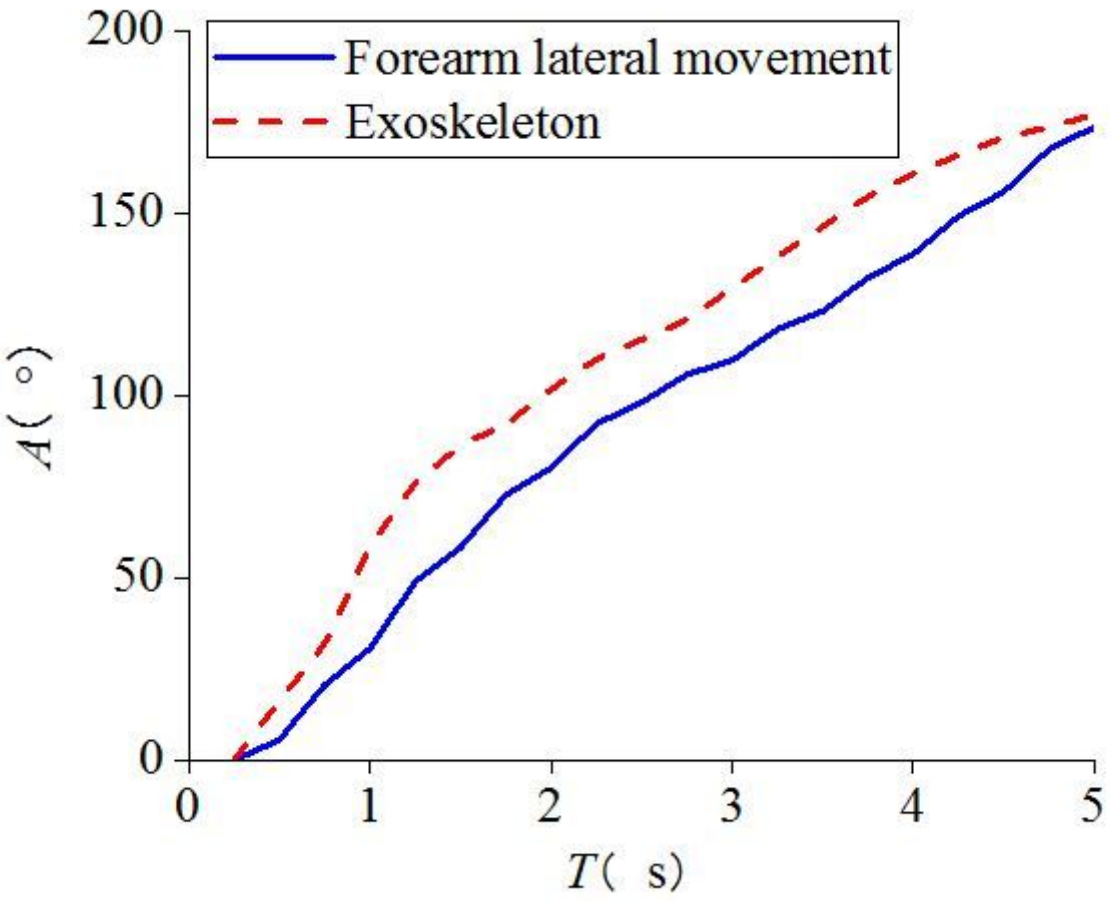


**Figure 7**

Tracking result of forearm lateral movement DOF

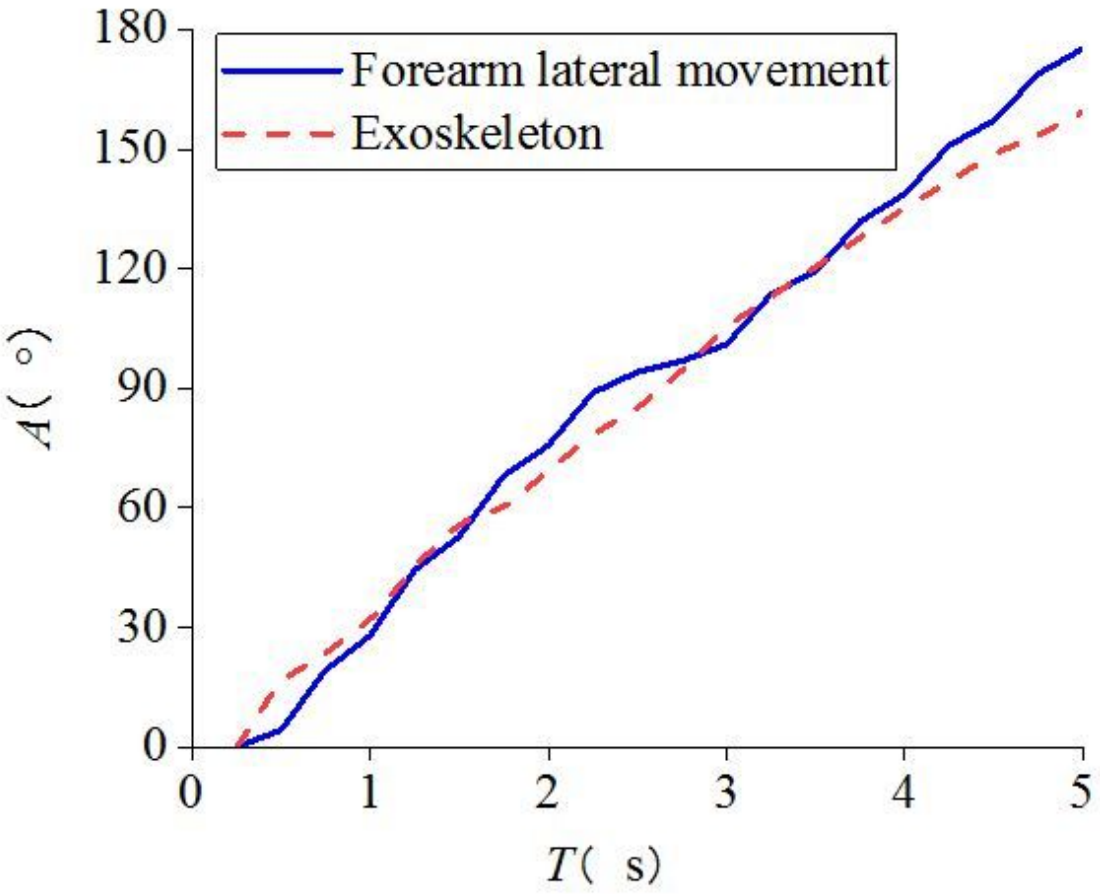


**Figure 8**

Subject 1 tracking results of forearm lateral movement DOF

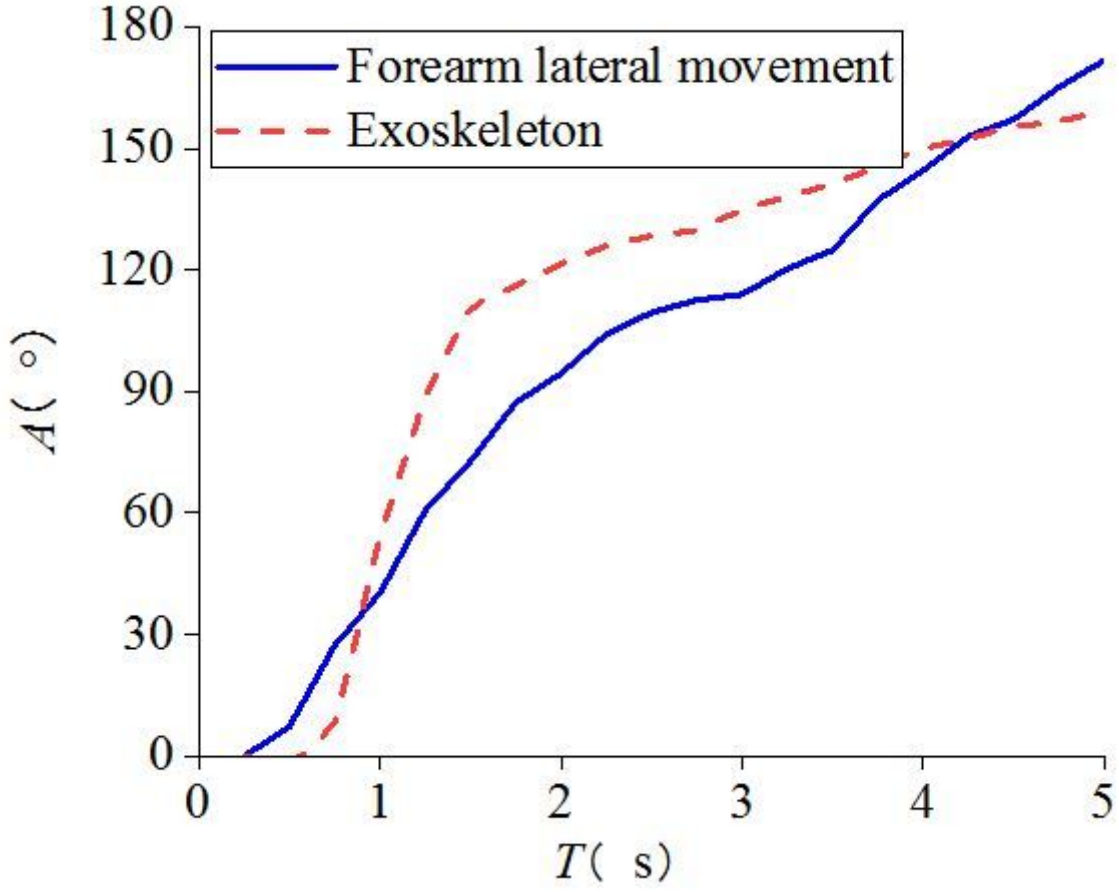


**Figure 9**

Subject 2 tracking results of forearm lateral movement DOF

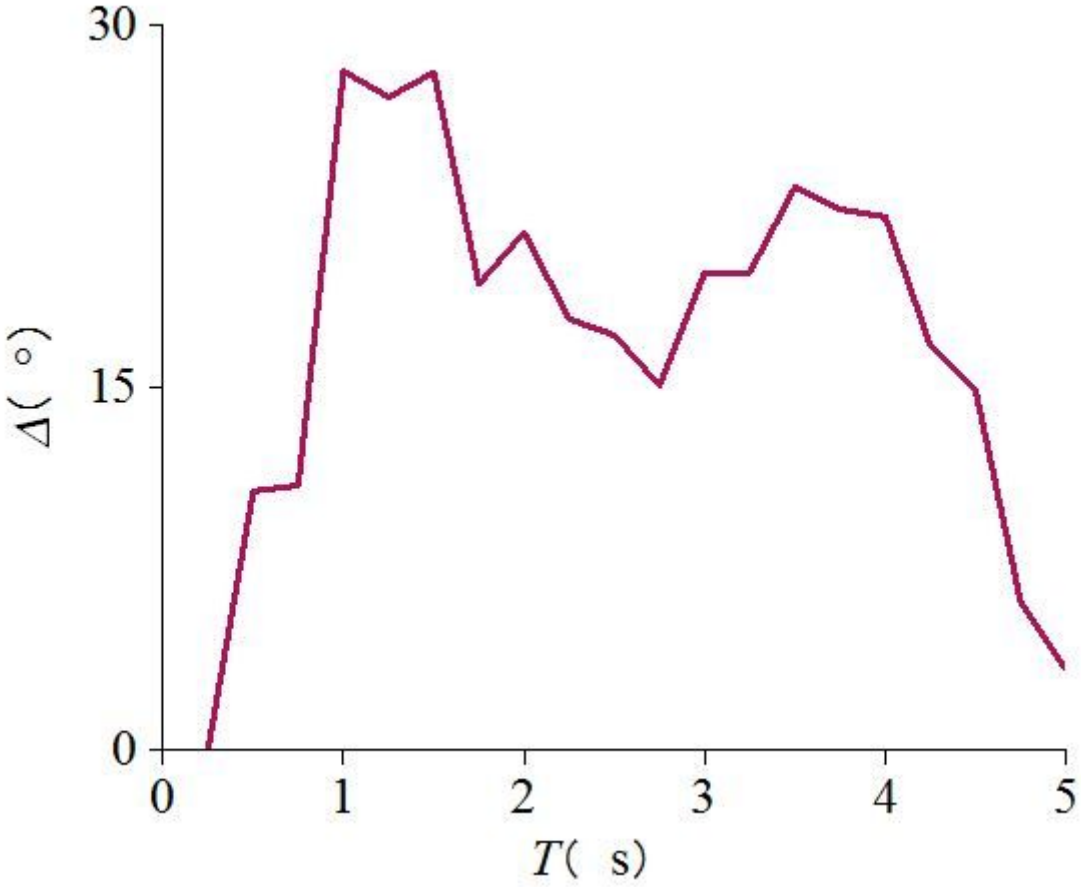


**Figure 10**

Absolute error curve of forearm lateral movement DOF

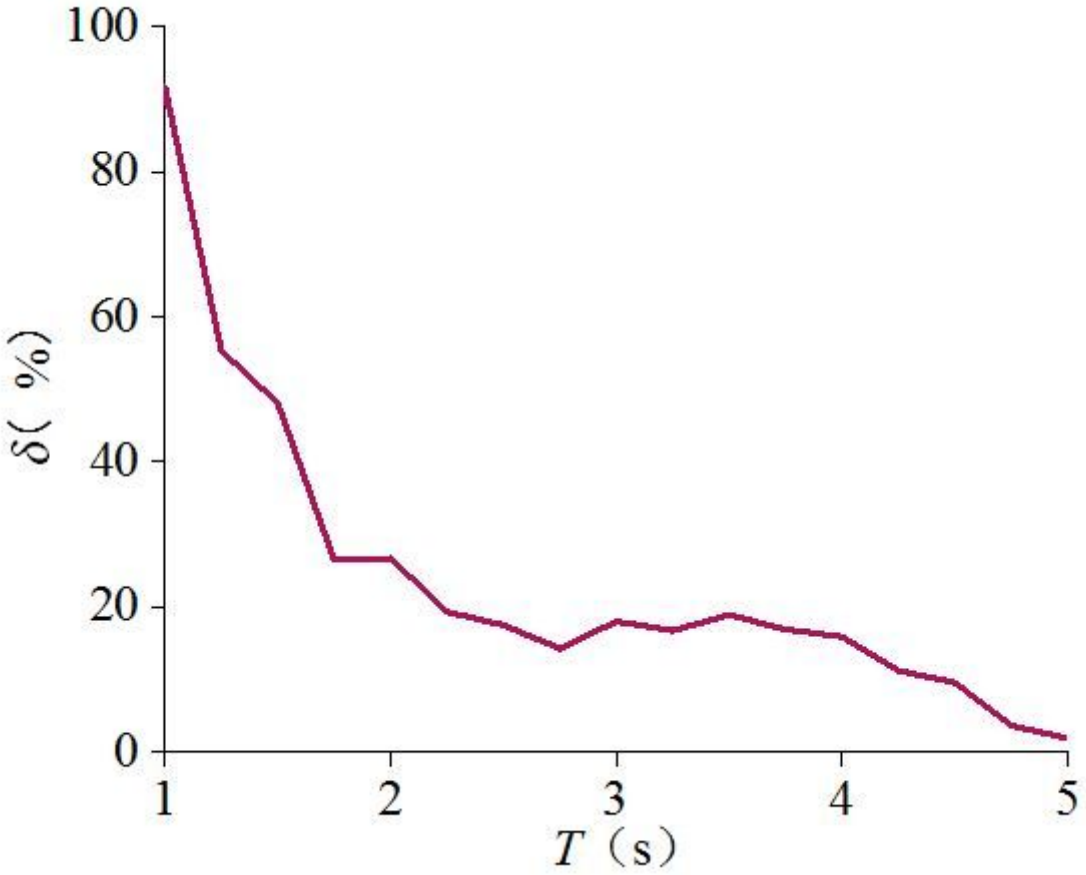


**Figure 11**

Relative error curve of forearm lateral movement DOF

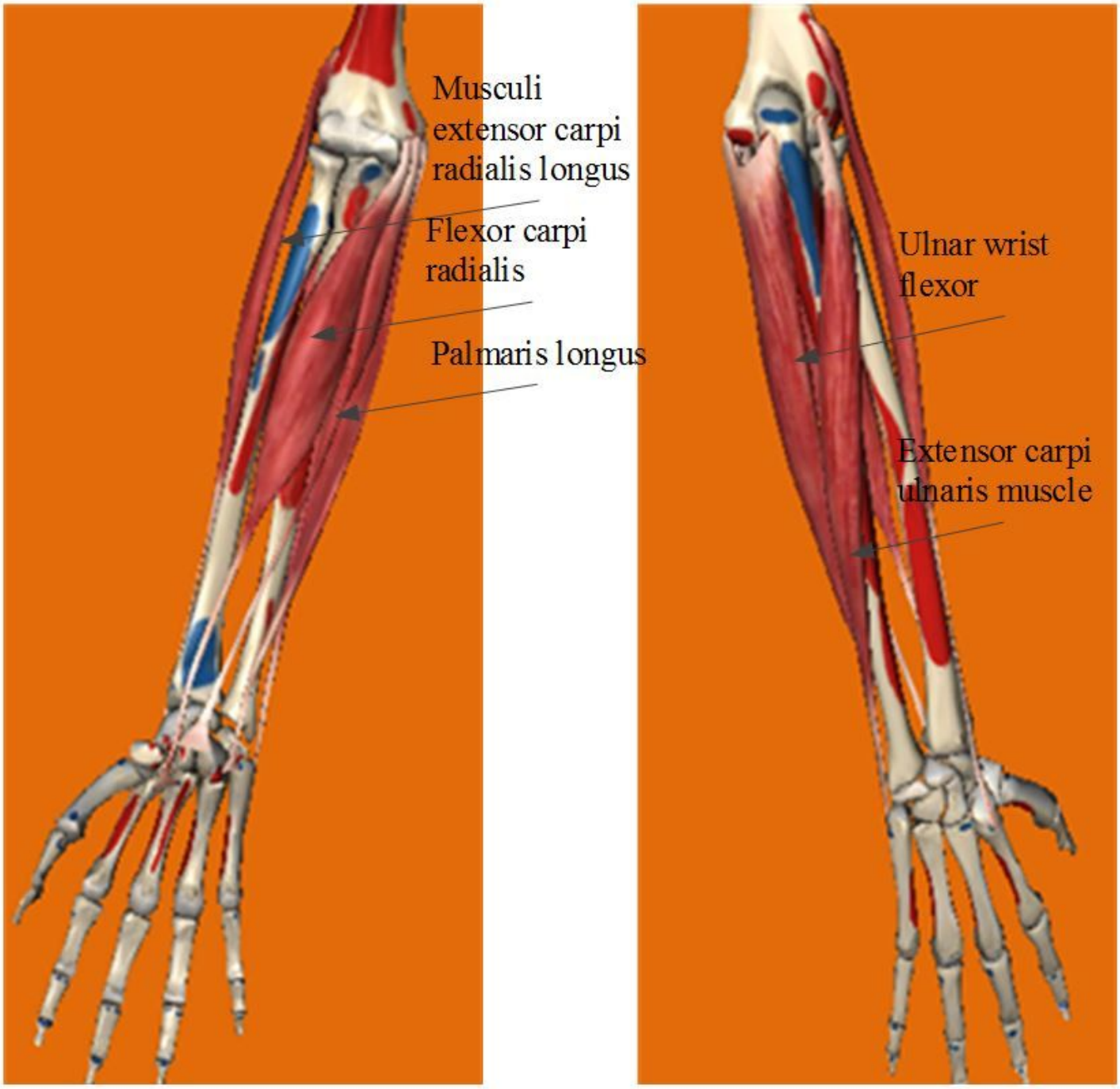


**Figure 12**

Selected muscles of wrist test

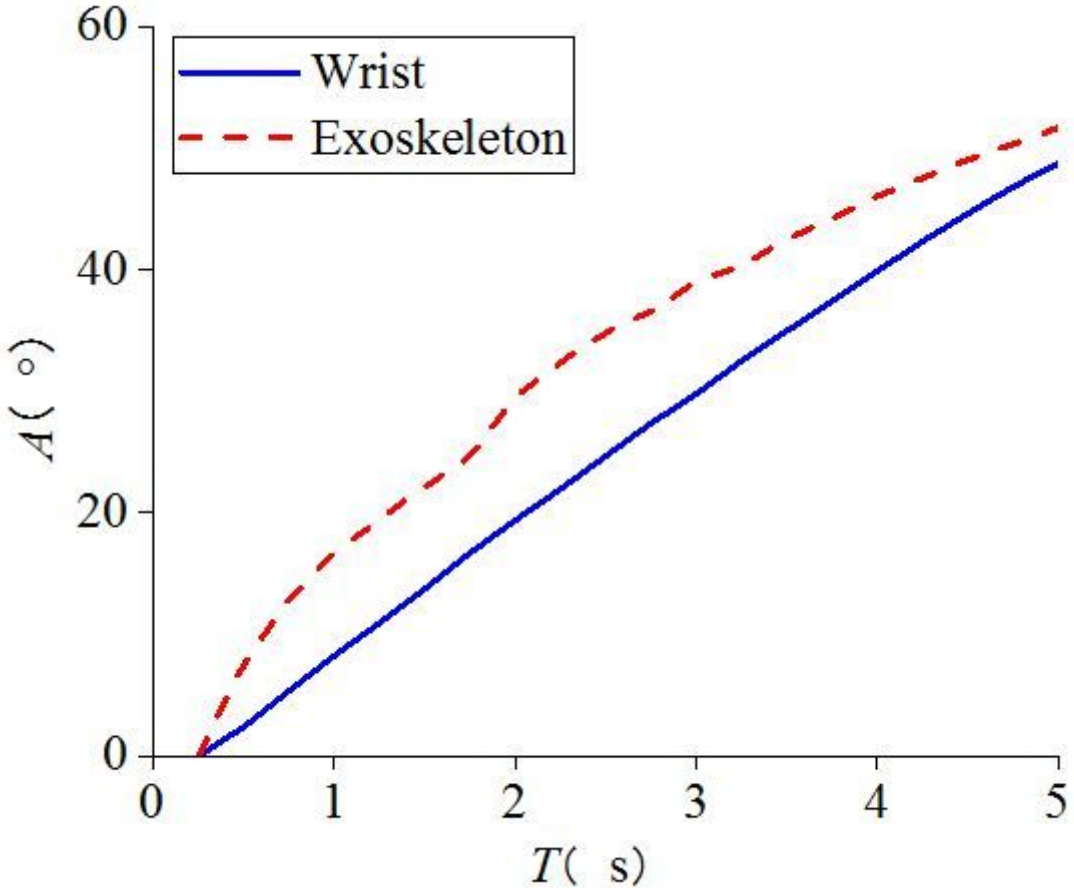


**Figure 13**

Tracking results of wrist swing DOF

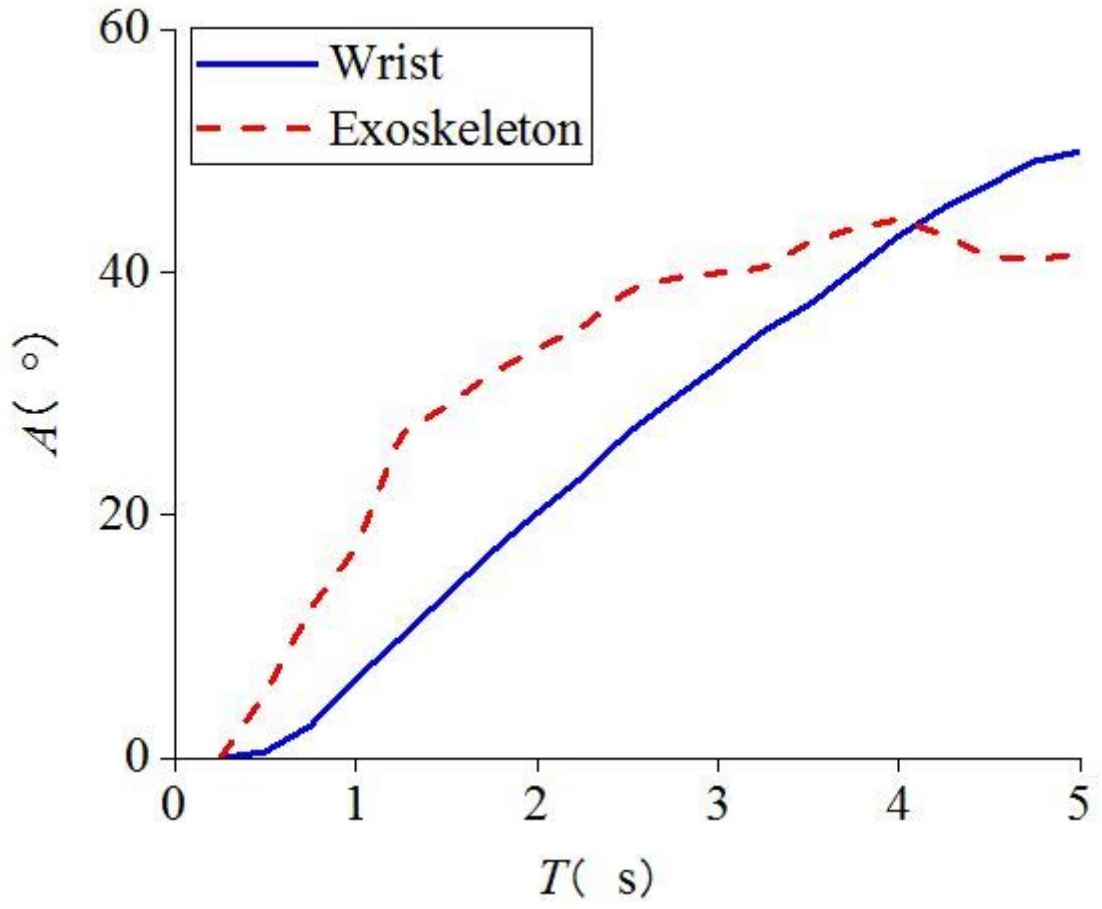


**Figure 14**

Subject 1 tracking results of wrist swing DOF

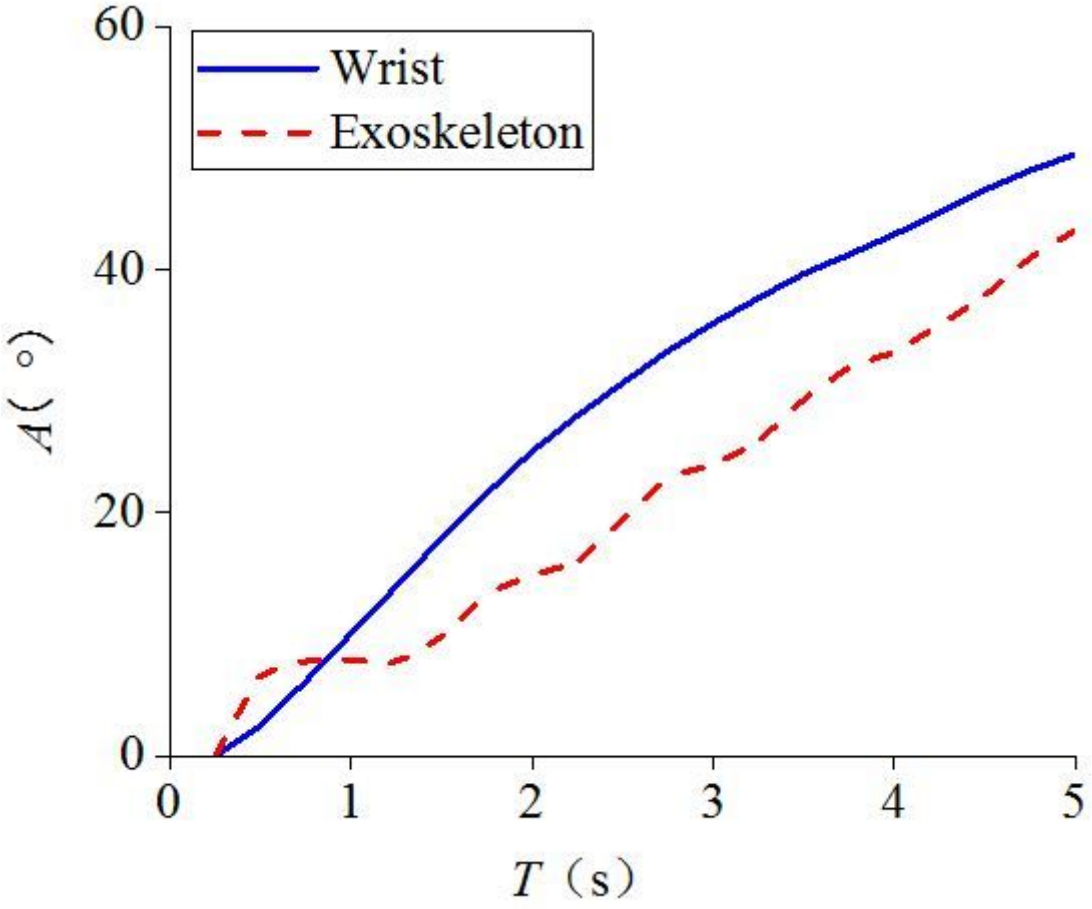


**Figure 15**

Subject 2 tracking results of wrist swing DOF

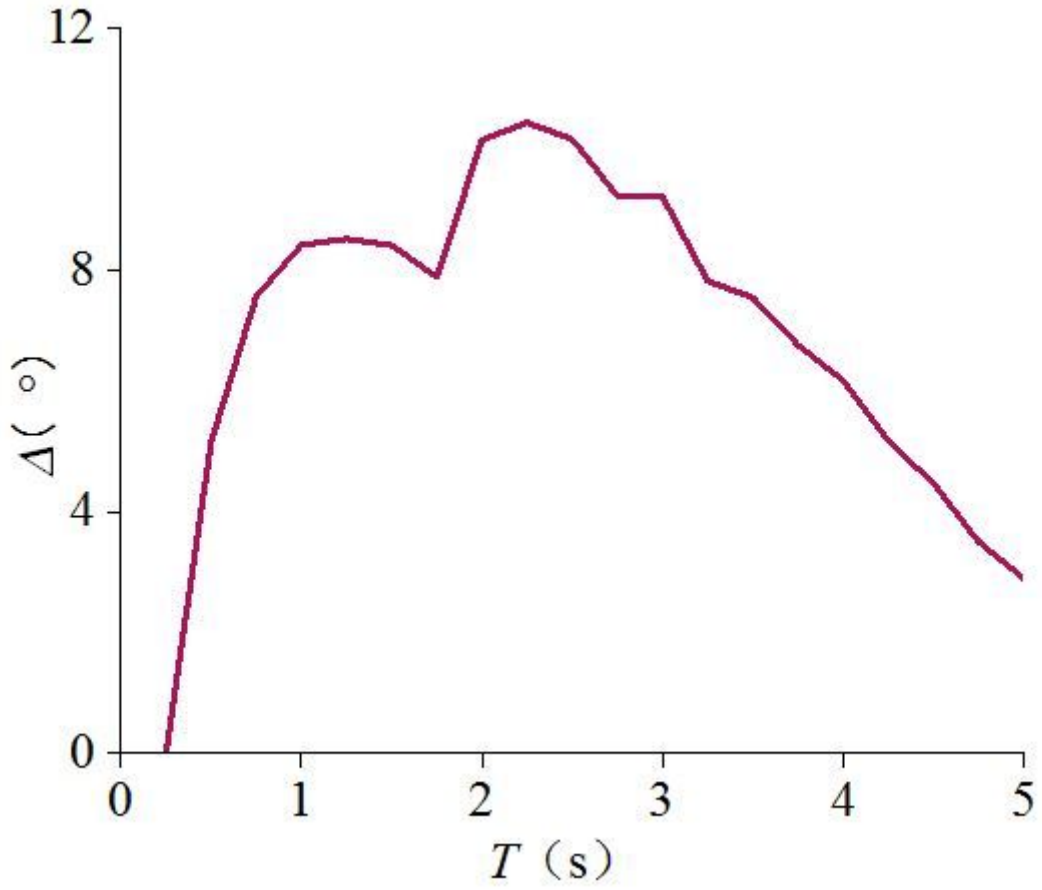


**Figure 16**

Absolute error curve of wrist swing DOF

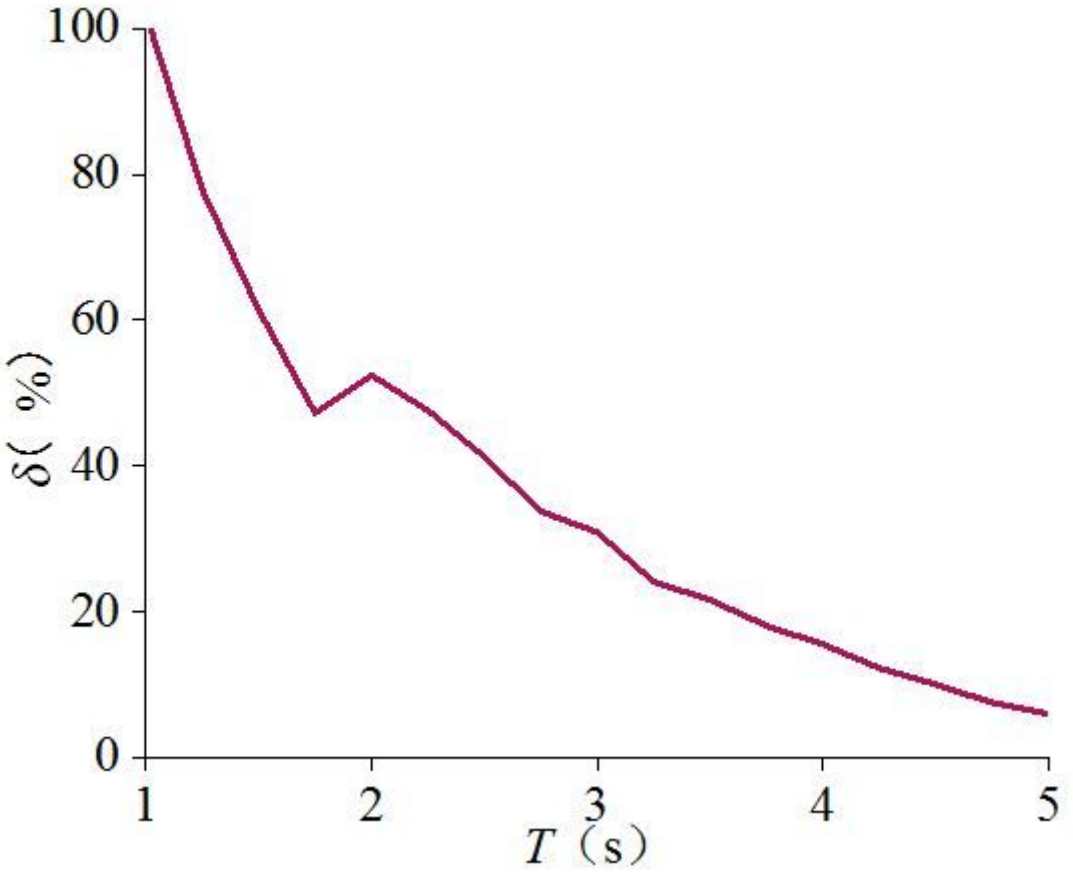


**Figure 17**

Relative error curve of wrist swing DOF